Edgar Andres Monterroso Urrutia

DETERMINATION OF BURNUP OF NUCLEAR FUEL

Master's thesis

Lappeenranta-Lahti University of Technology LUT
School of Energy Systems
Nuclear Engineering

University of Ljubljana
Faculty of Mathematics and Physics
Department of Physics
Nuclear Engineering

Supervisors: Prof. DSc. Juhani Hyvärinen
Prof. Dr. Luka Snoj

Ljubljana, 2021

ABSTRACT

Lappeenranta-Lahti University of Technology LUT
School of Energy Systems
Master's program in Energy Technology
Edgar Andres Monterroso Urrutia
DETERMINATION OF BURNUP OF NUCLEAR FUEL
Master's thesis
2021
88 pages, 25 figures and, 20 tables
Supervisors: Prof. DSc. Juhani Hyvärinen
Prof. Dr. Luka Snoj

Keywords: Gamma spectrometry; Fuel elements; Research reactors; Fission products; Fuel burnup

The concept of nuclear fuel burnup is introduced alongside some of its main applications. The fuel burnup equations are developed for its theoretical estimation and the gamma spectrometry technique is introduced as part of the non-destructive assays with its advantages, disadvantages and fuel burnup monitor selection, for its experimental estimation. A High-Purity Germanium detector from the "Jožef Stefan" Institute in Slovenia, was calibrated in energy and efficiency. Lastly, a Matlab code for the spectrum analysis was developed.

Contents

List of Figures

List of Tables

List of abbreviations and symbols

Abbreviation

The following abbreviations were mentioned throughout this work:

BUC burnup credit

ERI Relative Intrinsic Error

FE fuel element

FWHM Full with at half maximum

HPGe High-Purity Germanium

ICF isotopic correction factor

IJS Institut ”Jožef Stefan”

NDA non-destructive assay

NIST National Institute of Standards and Technology

Symbols

The following symbols, notations and units, were used to characterize the physical quantities mentioned throughout this work:

A_0	Initial activity from the certified calibration source (kBq)
a	Total counts recorded over the active part of the fuel element
A_E	Experimental activity (Bq)
α	Capture-to-fission ratio
A_T	Theoretical activity (Bq)

B_E	Experimental burnup (g)
B_T	Theoretical burnup value (g)
BU	Burnup
$BU_{\%}$	Burnup given in percentage
B_z	Axial geometrical buckling factor
C_c	total counts from the measurements taken during the calibration
C_i	Total counts from the i-th measurement over the fuel element
χ^g	Diffusion spectrum in the energy group g
D^g	Reactor diffusion constant
D_s	SS-304 cladding thikness from the fuel element
E_γ	Characteristic gamma ray energy (keV)
ϵ_e	Experimental detector intrinsic efficiency
ϵ_{ea}	Experimental detector absolute efficiency
$\epsilon_{e,c}$	Calculated detector intrinsic efficiency
F	fission density
f_a	self-attenuation coefficient
f_d	Decay of burnup monitor correction factor
F_p	Power correction factor
f_v	Environmental attenuation coefficient
G	Geometrical correction factor
I_c	Gamma ray emission intensity from the calibration sources
I_γ	Gamma ray emission intensity
k	reactor multiplication factor
L	Collimator tube total length (cm)
L_b	Bottom cap from the collimator tube (cm)
L_w	Distance from the fuel element to collimator tube when submerged in water (cm)
λ_x	Decay constant of the x fission product (s^{-1})
λ_c	Decay constant from a calibration source (s^{-1})
m	Total amount of positions where the fuel element was present
m_{HM}	Heavy metal mass
m_u^0	^{235}U initial mass (g)
M_u	^{235}U atomic weight
m_u	^{235}U consumed mass (g)
μ_a	Dry-air at sea level attenuation coefficient (cm^{-1})

μ_{fe}	U-ZrH fuel element attenuation coefficient (cm^{-1})
μ_{ss}	Stain-less steel attenuation coefficient (cm^{-1})
μ_w	Water attenuation coefficient (cm^{-1})
n	Total number of irradiation periods during the whole irradiation history of the fuel element
N_A	Avogrado number. 6.022×10^{23} (mol^{-1})
N_{act}	Number of actinides atoms from a specific fission product (atoms)
N_{fp}	Number of atoms from a specific fission product (atoms)
N_u^0	^{235}U initial number of atoms in the fuel element (atoms)
N_u	Concentration of ^{235}U (atoms/cm^3)
ν^g	Number of fission neutrons in the energy group g
N_x	Concentration of the x fission product (atoms/cm^3)
$N_{x,e}$	Experimental concentration of the x fission product (atoms/cm^3)
P_i	Average relative power corresponding to the i-th irradiation position
P_k	Average relative power corresponding to the k-th irradiation period
$P(t)$	Power as function of time
ϕ^g	Neutron flux from energy group g (neutrons/cm^2-s)
ϕ	Neutron flux (neutrons/cm^2-s)
$\phi(E)$	Energy dependent neutron flux
q	Total amount of measurement done over the active part of the fuel element
r_d	Calibration collimator tube radius (cm)
R_i	U-ZrH fuel element meat internal radius (cm)
R_o	U-ZrH fuel element meat external radius (cm)
r_{sd}	Calibration source-detector distance (cm)
$\Sigma^{g' \to g}$	scattering cross-section from energy group g' to group g
Σ_f^g	Fission cross section for the energy group g
Σ_r^g	Removal cross-section
σ_u^f	Fission microscopic cross-section of ^{235}U (cm^2)
σ_x^c	Capture microscopic cross-section of the x fission product (cm^2)
$\sigma^x(E)$	Energy dependent cross section for the x reaction type
$T_{1/2}$	Half-life (s)
τ_k	Time interval between the end of the k-th irradiation period and the end of the last irradiation period (s)
t_c	Counting time for the calibration spectrum acquisition (s)
t_d	Cooling-down time of the fuel element outside from the reactor core (s)

$t_{c,i}$	Total acquisition time for the C_i measurement (s)
t_i	Total irradiation time for the fuel elements (s)
t_k	Duration of the k-th irradiation period (s)
V_{fe}	Active fuel volume from the fuel element (cm^3)
Y	Average fission yield ($\%$)
Y_x	Fission yield of a the x fission product
Y_{fp}	Fission yield from a specific fission product

Chapter 1

Introduction

From the beginning of the operation of the 250 kW TRIGA Mark II research reactor at the Institut "Jožef Stefan" (IJS) in 1966, the analysis of the degree of burnup of the irradiated fuel elements (FEs) has been made by means of deterministic neutron calculations by using unit cell and diffusion codes and, in more recent times, with Monte Carlo neutron transport simulations, nevertheless these calculations would benefit from experimental verification [1].

Gamma spectrometry in irradiated fuel elements is a technique used to evaluate the validity and reliability of the theoretical calculations since the experimental results it provides can be directly compared with those predicted by neutronic calculations or a previously validated Monte Carlo simulation. In addition, with this non-destructive analysis, it is possible to obtain the burnup geometrical profiles for the individual FEs

In the following work, the main methods to determine fuel burnup on FEs by experimental means are presented, giving special attention to the gamma spectrometry technique and all the considerations concerning said technique.

1.1 Objectives

The general, as well as the specific objectives that were established to carry out the following work at the TRIGA Reactor in the IJS are indicated below.

1.1.1 General

To conduct a research in the area of nuclear engineering, presenting the different methodologies for fuel burnup determination and, establishing a methodology that allows the determination of the degree of burnup using experimental techniques at the TRIGA reactor at the IJS.

1.1.2 Specific

- Present the different experimental methodologies for fuel burnup determination with focus on gama spectrometry as a very accurate non-destructive method.
- Present a more detailed analysis for the gamma spectrometry technique. Give the advantages and disadvantages over the rest of the methods and;
- Present a generalized procedure for the application of the gamma spectrometry technique over a FE, for the fuel burnup determination.
- Characterize a high resolution gamma spectrometry system at the IJS, by determining energy calibration and efficiency calibration under laboratory conditions.

1.2 Basic Concepts

In this section some basic concepts from reactor physics and gamma spectrometry analysis are introduced.

1.2.1 Plural modes of attenuation

"Linear attenuation coefficient (μ) is a constant that describes the fraction of attenuated incident photons in a mono-energetic beam per unit thickness of a material. It includes all possible interactions including coherent scatter, Compton scatter and photoelectric effect. It is expressed numerically in units of cm^{-1}. The linear attenuation coefficient increases

with increasing atomic number and increasing physical density of the absorbing material. It decreases with increasing photon energy" [2].

When μ is divided by the density (ρ) of the attenuation medium, the mass linear attenuation coefficient (μ/ρ) is obtained. For a general case, where several elements are present the attenuation coefficient is defined as

$$\mu = \sum_{i=1}^{n} w_i \cdot \mu_i \tag{1.1}$$

Where μ_i is the linear attenuation coefficient for the element i given in 1/cm and, w_i is the weight percentage of the element i.

1.2.2 Cross section

"Is defined as the probability that a given atomic nucleus or subatomic particle will exhibit a specific reaction (for example: absorption, σ_a; scattering σ_s; fission, σ_f; radiative capture, σ_c) in relation to a particular species of incident particle" [3].

The cross section, is expressed in terms of area. Due to the usual small values the unit barn (b) is defined. Where, 1 b = 10^{-24} cm^2. Since there is a cross section value for each possible type of interaction, the total cross section is defined as

$$\sigma_t = \sigma_a + \sigma_s + \sigma_f + \sigma_c + ... \tag{1.2}$$

The total cross section measures the probability that an interaction of any type will occur when a particle hit the target. When a cross section σ of a determined process is applied to an individual nucleus is known as the microscopic cross section. Since the material acting as target has a density D of nuclides per cm^3, the quantity $D\sigma_t$ receive the name of the total macroscopic cross section and, is represented by Σ. The total macroscopic cross section of a mix of elements is given by

$$\Sigma_{mix} = \Sigma_1 + \Sigma_2 + ... \tag{1.3}$$

1.2.3 Neutron flux

"A measure of the intensity of neutron radiation, determined by the rate of flow of neutrons. The neutron flux value is calculated as the neutron density (D) multiplied by neutron velocity (v), expressed in centimeters per second, or cm/sec. Consequently, neutron

flux (Dv) is measured in neutrons/cm^2-sec" [4].

In an actual thermal nuclear reactor there is a great quantity of thermal neutrons that are constantly changing energy due to the thermalization process, that which produces a distribution in energies that is represented by the Maxwell-Boltzmann distribution law of the general theory of gases, that is represented by

$$\frac{n(E)}{n_{th}} = \frac{2\pi}{(\pi kT)^{3/2}} e^{-E/kT} E^{1/2} \tag{1.4}$$

where, n(E) is the amount of neutrons with energy E, n_{th} is the total amount of thermal neutrons, T is the absolute temperature (ºK) and the Boltzmann constant given by $k = 8.617 \times 10^{-5}$ (eV/K). From this distribution law it can be deduced that the average neutron kinetic energy is given by $\overline{E} = (3/2)kT$ and the most probable kinetic energy is kT. This implies that for the particular case of the thermal neutrons the most probable energy is 0.025 eV. From this kinetic energy, the most probable velocity can be determined, given by

$$v = \sqrt{\frac{2kT}{m_n}} \tag{1.5}$$

where m_n is the mass of the neutron given by 939.6 (MeV/c^2) and, for the case of this thermal neutrons the temperature is 294 ºK. Therefore, the most probable velocity is 2210 (m/s). Thus, it can be concluded that for the particular case of the thermal neutrons, the thermal flux can be expressed as

$$\phi_{th} = n_{th} \cdot v_{th} \tag{1.6}$$

This thermal flux is comprised for energies ranging from 0 eV to 0.5 eV, meanwhile the neutrons with an energy between 1 eV and 100 keV are considered as epithermal neutrons and, above 100 keV they become fast neutrons.

1.2.4 Reaction rate

The reaction rate (RR) is defined as the number of interactions taking place in a volume per unit of time. In a general form is given by [5],

$$RR = \int \sigma^x(E)\phi(E)dE \tag{1.7}$$

where $\sigma^x(E)$ is the energy dependent cross section for the x reaction type and $\phi(E)$ is the energy dependent neutron flux. The fission reaction rate for mono-energetic thermal neutrons is then given by

$$RR_f = \phi_{th}\Sigma_{f,th} \tag{1.8}$$

1.2.5 Power

In a reactor with an active fixed volume V, the power due to fission is given by [5],

$$P = \epsilon_f \cdot V \cdot \int \sigma^f(E)\phi(E)dE \tag{1.9}$$

where ϵ_f is the average energy release per fission (≈200 MeV = 3.2044×10^{-11} J). For mono-energetic thermal neutrons the above equation becomes,

$$P = \epsilon_f \cdot V \cdot \phi_{th}\Sigma_{f,th} \tag{1.10}$$

Therefore, in a determined active reactor volume where the fissions are produced by neutrons in a defined energy interval, the power is proportional to the product of the fission macroscopic cross-section times the neutron flux, i.e. the reaction rate.

1.2.6 Gamma spectrometry

When an unstable atomic nucleus decays into a more stable nucleus, the "daughter" nucleus is sometimes produced in an excited state. The subsequent relaxation of the daughter nucleus to a lower-energy state results in the emission of a gamma-ray photon. Gamma-ray spectrometry, involving the precise measurement of gamma-ray photon energies emitted by different nuclei, can establish nuclear energy-level structures and allows for the identification of trace radioactive elements through their gamma-ray emissions [6].

When these gamma emissions are detected and analyzed in a spectrometry system, a gamma ray spectrum can be produced. Each of this spectrum is characteristic for the emitting gamma rays from the nuclide.

In summary, is a nuclear technique used to determine and quantify the radioactive isotopes on a sample by means of counts vs. energy frequency distribution histogram.

1.2.6.1 Gaussian distribution

Is a type of continuous probability distribution for a real-valued random variable, given by [7]:

$$P_G(E; E_\gamma, \sigma) = C_N \int_{-\infty}^{\infty} \frac{1}{\sigma\sqrt{2\pi}} exp\left[\frac{-1}{2}\left(\frac{E - E_\gamma}{\sigma}\right)^2\right] dE \tag{1.11}$$

Since the probability is normalized, C_N is the area under the curve; i.e., the photo-peak total counts from the spectral analysis, σ is the standard deviation, E_γ is the displacement parameter that specifies the location of the peak at the center of the distribution; i.e., the characteristic gamma energy of the nuclide. The previous definition assumes that the background from the spectrum is negligible or it would be somehow removed.

It is possible to characterize a distribution by its Full-With-at-Half-maximum (FWHM) Γ, defined as the range of E between values at which the probability is half its maximum value and is related with the standard deviation σ by,

$$\Gamma = 2.354 \cdot \sigma \tag{1.12}$$

The most common way of displaying pulse amplitude information is through the differential pulse height distribution, see Figure 1.1.

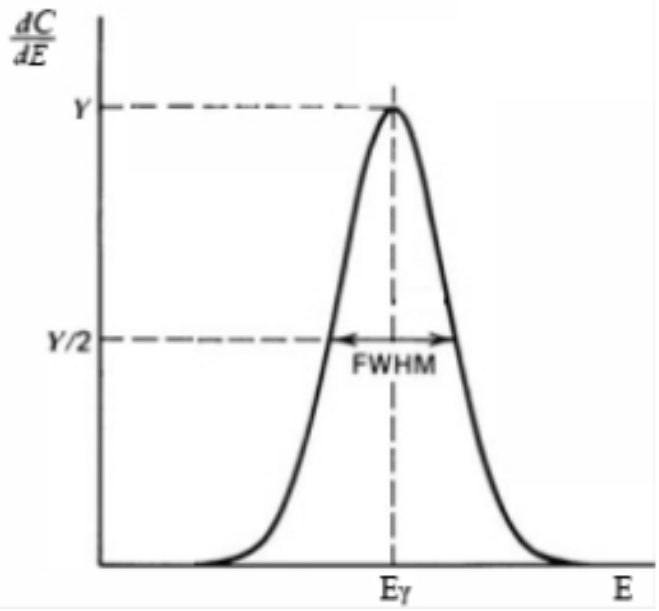

Figure 1.1: Differential pulse height distribution. Where dC/dE are the counts per Energy E and, Y indicates the total height of the spectra [8].

1.2.6.2 Energy resolution

Resolution is the ability of the gamma spectrometry system to resolve (distinguish) between nearby energies of incident gamma rays [9].

The main objective of the gamma spectrometry technique is the measurement of the photo-peak area for each spectrum. The precision with which this can be achieved depends on the resolution, R, which is defined as [8],

$$R = \frac{\text{FWHM}}{E_\gamma} \tag{1.13}$$

where FWHM is the abbreviation of Full-Width-at-Half-Maximum, see Figure 1.1.

1.2.6.3 Detection efficiencies

It is convenient to subdivide counting efficiencies into two classes: absolute and intrinsic. Absolute efficiency is defined as [8],

$$\epsilon_{abs} = \frac{\text{number of pulses recorded}}{\text{number of radiation quanta emitted by source}} \tag{1.14}$$

ϵ_{abs} is dependent of the detector properties and, also of the counting geometry (primary of the distance from the source). Intrinsic efficiency is defined as

$$\epsilon_{int} = \frac{\text{number of pulses recorded}}{\text{number of radiation quanta incident on detector}} \tag{1.15}$$

and no longer includes the solid angle subtended by the detector as an implicit factor. The two efficiencies are simply related for isotropic sources by

$$\epsilon_{abs} = \epsilon_{int} \left(\frac{\Omega}{4\pi} \right) \tag{1.16}$$

where Ω is the solid angle of the detector seen from the actual source position.

1.2.7 Semiconductor detectors

Semiconductors properties are described by means of the solid state band structure due to their crystalline structures. In crystals, electrons can occupy two possible energy levels, those low energy levels in which electrons are bound to the crystal lattice and cannot move freely, are known as the valence band, while the energy levels with the highest energy

where electrons move freely are known as the conduction band. Between the valence band and the conduction band there are forbidden energy levels, which are known as the forbidden band. Electrons can move from the valence band to the conduction band when enough thermal or electromagnetic energy is applied to overcome the gap of the forbidden band, this event produces an absence of electron in the valence band that is known as a hole and which is considered as a positive charge. The electron of the conduction band together with the gap of the valence band is known as an electron-hole pair [10].

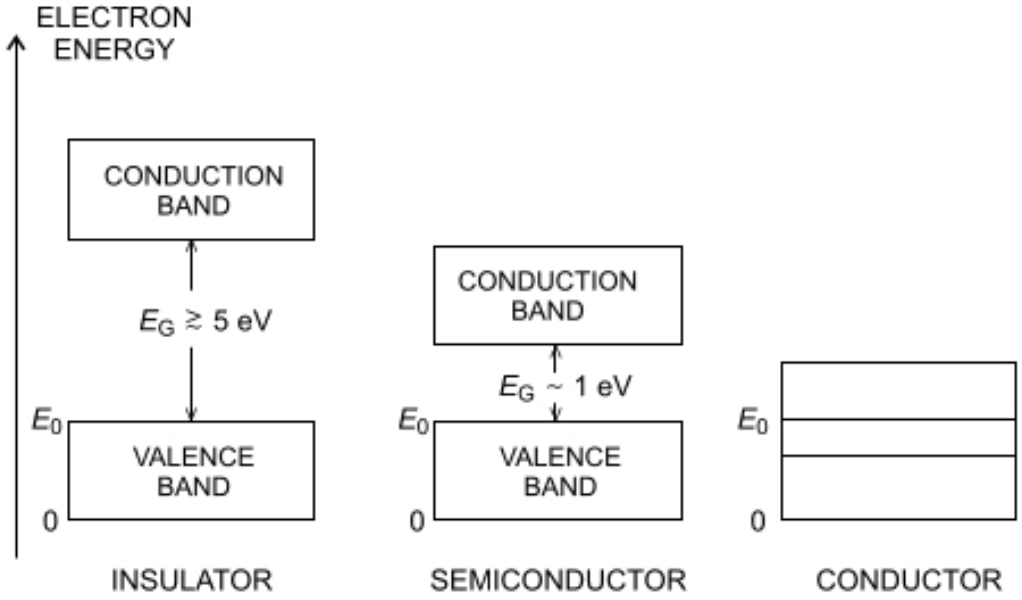

Figure 1.2: Band structure of insulators, semiconductors and, conductors. The energy at the top of the valence band is denoted by E_0 and E_G is the size of the band gap [10].

The basic principle of operation of the semiconductor detectors is the production of electron-hole pairs as charge carriers through the interaction of radiation with the semiconductor material. Germanium (Ge) and silicon (Si) are the main materials used as semiconductor detectors [8].

The main characteristics of semiconductor detectors are [9]:

- Compact and solid structure.
- High efficiency for electromagnetic radiation.
- The formation time of the output pulses is a few nanoseconds.
- Linear response over a wide range of energy.
- High resolution in energy.

1.2.7.1 Germanium detectors

Semiconductor detectors are advantageous in gamma spectrometry applications as they have better resolution. In these detectors, charge carriers are produced mainly by the change in temperature and by the radiation that interacts with the semiconductor material. Germanium has a relatively small band gap energy, 0.67 eV at 300ºK, which cause the semiconductor crystal to stop function properly and lose its properties for purposes of gamma spectrometry. For this reason, it is essential to maintain this type of detectors at liquid nitrogen temperatures to avoid directly affecting the resolution of the detection system [8, 11].

With the advances in the techniques for the purification of germanium, it was possible to introduce hyper-pure germanium detectors (HPGe), which have the advantage that they can be kept at room temperature when not in operation. Germanium has a high atomic number, which provides an advantage in the detection of gamma radiation since the probability that electromagnetic radiation interacts through the photoelectric effect is proportional to Z, therefore germanium has a superior advantage over silicon. Another advantage of germanium detectors is that they can have high efficiencies, as well as that they have much better resolution than silicon-lithium and surface barrier detectors [12].

Figure 1.3: Examples of HPGe detectors by Canberra, Inc [10].

1.2.8 Propagation of uncertainties

When several quantities x_1, ..., x_j are measured with small independent uncertainties δx_1, ..., δx_j, and these values are used to calculate a quantity Q, then the uncertainty in Q is calculated as follows [13]

$$\delta Q = \sqrt{\left(\frac{\partial Q}{\partial x_1}\delta x_1\right)^2 + ... + \left(\frac{\partial Q}{\partial x_j}\delta x_j\right)^2} \tag{1.17}$$

Chapter 2

Fuel burnup

Nuclear fuel burnup is defined as the total energy released in fission divided by mass of fuel i.e., only fissile and fissionable material, often refereed to as the heavy metal. It is usually expressed in units of Megwatt-days per metric ton of heavy metal and is mathematically defined as [14],

$$BU = \frac{\int P(t)dt}{m_{HM}} \tag{2.1}$$

where BU is the burnup, $P(t)$ is the power as function of time and, m_{HM} is the heavy metal mass.

The burnup of nuclear fuel can be considered as a way of measuring the amount of uranium from the fuel that was consumed during irradiation inside the reactor core and this measure would be equal to the amount of energy produced by this uranium. To be able to compare the estimated values with the ones obtained experimentally the fuel burnup can be presented in grams of $^{235}\mathrm{U}$ consumed from the fuel elements. 1 MWd = 8.64×10^{10} J corresponding to the fission of approximately 1.05 g of $^{235}\mathrm{U}$ [15].

At a nuclear reactor the fuel is subjected to significant restructuring processes determined by neutron irradiation directly through nuclear reactions, indirectly through the thermo-mechanical conditions established as a consequence of such reactions and, by the fission products that are created inside the fuel [15, 16].

2.1 Why to do burnup calculations?

What was mentioned above, give rise to the following question: Until when is it possible to subtract energy from the fuel in the form of heat? From an economical point of view, the ideal case, would be until the total amount of uranium would be completely depleted from the FE but, due to several phenomena affecting the FE, such as: thermal performance, fuel chemistry, swelling due to fission gases, radiation damage, hardening, embrittlement, irradiation creep, etc. limitations arise during its operational life inside the core that need to be taken into account [17].

Nevertheless, depending on what is wanted to be achieve, burnup calculation will be done the same way but the results will have different scopes. While the most common objective is related to the estimation of the energy released in the fuel, is not limited to it. Can also be used to establish strategic planning for fuel management including reshuffling and reloading schemes patterns and also, as an integral part of safety and safeguards analysis.

In the following sections a brief, but concise, explanation of some of the main different applications for the fuel burnup analysis are given.

2.1.1 Fuel economics

The procurement, fabrication, utilization, reprocessing after said utilization and, disposal of the nuclear fuel; all together comprehend what is know as the nuclear fuel cycle. The nuclear fuel cycle is subdivided in two main parts known as: the front-end and the back-end. The front-end is related to all the events happening, before and during, the utilization of the nuclear fuel. Meanwhile, the back-end is related to the events happening after the fuel is removed from the core [18, 19].

A general overview of the main parts of a closed uranium fuel cycle:

- Front-end
    1. Mining.
    2. Concentration (or milling).
    3. Conversion.
    4. Enrichment. Including isotope separation.
    5. Fabrication.

6. Fuel usage. In-core fuel management.

- Back-end

7. Spent fuel storage and decay.

8. Reprocessing.

9. Waste disposal.

Among the elements of the front-end, is the in-core fuel management that deals on how to get as much energy as possible while using as little fuel as possible without passing any safety limit. An effort to satisfy the previous objective leads to an optimization problem where fuel and core designers try to obtain a balance between fuel economics and safety limits.

Since in a typical core, the core size, fuel assembly design, control devices and coolant conditions will be fixed, the possibility of addressing the optimization problem should be focus on some general considerations: the type of fuel, the operation strategy, the fuel distribution inside the core, the number of loading patterns, *the level and profile of enrichment of the fuel*, the mechanical elements of the fuel, the use of the control rods and, who and how design the reactor.

2.1.2 Safety analysis

Neutron multiplication is driven by the production and loss of neutrons. In a finite system, such as a spent fuel cask, the peak neutron multiplication occurs at a location where neutron production is maximized while loss is simultaneously minimized. The axial variation in flux due to the burnup distribution, is dependent upon the accumulated burnup, as well as other characteristics of the assembly operating history and is influenced by the presence of actinide and fission product absorbers, since they tend to reduce reactivity. This would have a direct effect in the *burnup credit*, defined as the credit take for the reduction of reactivity due to fuel burnup [20].

In the past, criticality safety analyses for spent fuel storage and transport cask, assumed the spent fuel to be fresh (unburned) fuel with uniform isotopic corresponding to the maximum allowable enrichment. In order to optimize this conservative approach, the burnup credit (BUC) methodology is developed.

Criticality safety analysis are performed to demonstrate that a proposed fuel storage or

transport configuration meets applicable regulatory requirements. The BUC methodology for a transport and storage cask application consists of the following important steps [21]:

- The definition of bounding conditions of irradiation, i.e., fuel history.
- The experimental validation of the used fuel inventory and the reactivity worth of the selected actinides and fission products. This validation is used to derive isotopic correction factor (ICF) terms in order to guarantee the proper calculations in the used fuel inventory.
- The determination of axial burnup profiles for criticality calculations.

These ICFs are key to guarantee the fuel reactivity in safety-criticality calculations using the BUC approach.

Additionally, fuel burnup is an important part of the nuclear spent fuel safety analysis, mainly for the source term analysis for safe handling and final disposal. Source term includes decay heat, nuclide inventory, reactivity and, photon emission rate, just to mention a few. For example, the estimation of decay heat and reactivity allows the estimation of the final disposal fuel canister maximum capacity and; the knowledge of nuclide inventory allows the safe handling of the spent fuel, from a radiation safety point of view [22].

2.1.3 Safeguards

The safeguarding of nuclear materials is a critical technical and political aspect of nuclear fuel reprocessing. Nuclear fuel reprocessing is one of the parts from the back-end of the nuclear fuel cycle. Simply defined, nuclear safeguards are measures used to verify that civil nuclear materials are properly accounted for and are not diverted to undeclared uses non-proliferation of nuclear weapons. For safeguard purpose nuclear material is specifically defined as either special fissionable material or source material. Special fissionable material is $^{239}\mathrm{Pu}$ or uranium enriched in either $^{235}\mathrm{U}$ or $^{233}\mathrm{U}$. Since how the fissile material is been used is one of the main interest of the safeguards, the measurement of the fuel burnup becomes essential [23].

2.2 TRIGA reactor nuclear fuel

The fuel of a typical TRIGA Mark reactor is contained within cylindrical fuel element rods made of stainless steel (SS-304) with a thickness of (0.051 $\pm$ 0.003) cm. The height of an individual element is 73.2 cm – the upper and lower end of the element are designed in such a way that they enable safe positioning in the core and possible remote manipulation from the reactor operator. The central part is cylindrically shaped. The fuel meat is in the form of a homogeneous mixture of uranium and zirconium hydride (U-ZrH) and has a pellet like structure. Three pellets are vertically stacked within the fuel element with no significant gaps between them – they have a combined height of 38.1 cm [24], see Figure 2.1.

The material composition for a fresh fuel with a low enrichment ($\leq$ 20%), when the burnup isotopic changes are not taken into account, can typically range for its weight percentages, between: U 8.5%-12%, Zr 86.53%-89.85% and, H 1.53%-1.65%; where all these quantities should add up to 100%. Other important quantities are the H/Zr atom ration that can range between 1-1.7 and, the average ^{235}U mass that can range between 38g-56g [12, 24].

The ZrH is used as a moderator because for this particular molecule the H behaves as a simple harmonic oscillator therefore, at low temperatures the H has a low kinetic energy, thus behaving as a good hydrogenated moderator, but at high temperatures the rise in kinetic energy provokes the loss of the moderating properties, since instead of slowing down the neutrons during the collisions, an energy increase creates leaks in the system and non-productive absorptions in the fuel. Due to this property, the fuel has a high negative prompt temperature reactivity coefficient, thus during a sudden increase in power, this temperature related property will result in a negative temperature coefficient and therefore make the TRIGA reactor inherently safe [12].

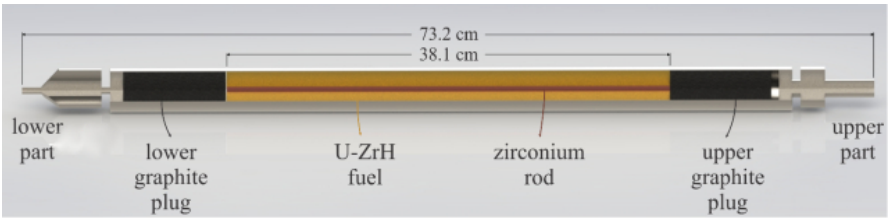

Figure 2.1: Cut view of the FE with the U-ZrH fuel. The diameters of the U-ZrH fuel part; i.e., the active part of the FE, are: outer (3.645 $\pm$ 0.008) cm and, inner (0.64 $\pm$ 0.01) cm. Where the inner diameter is equal to the zirconium rod diameter [24].

For the TRIGA Mark II research reactor at the IJS, the nuclide composition for an average FE is, see Table 2.1.

Table 2.1: Nuclide composition of an average fresh fuel element from the IJS TRIGA II reactor [24].

Component	Material	Content [wt%]	Density [g/cm^3]
Fuel	U-ZrH	100.0000	6.04495
	H	1.5298	
	Zr	86.5302	
	U	11.9400	
Cladding	SS-304	100.00	7.889
	Fe	66.84	
	Cr	19.00	
	Ni	10.00	
	Mn	2.00	
	Si	2.00	
	C	0.08	
	P	0.04	
	S	0.04	

2.2.1 Fission products

When fission of ^{235}U occurs, the fission products are produced in an asymmetric way, so that the masses of the two fragments are substantially different [19].

For ^{235}U isotope, the considered isotopes created from direct nuclear fission which can significantly affect the effective cross section of the fuel, by either absorption, scattering or fission reaction are [24, 25]: ^{79}Se, ^{83}Kr, ^{85}Kr, ^{85}Rb, ^{87}Rb, ^{88}Sr, ^{90}Sr, ^{95}Zr, ^{97}Zr, ^{99}Mo, ^{101}Ru, ^{103}Ru, ^{103}Rh, ^{106}Ru, ^{105}Rh, ^{107}Pd, ^{108}Pd, ^{109}Ag, ^{127}Sb, ^{129}I, ^{131}I, ^{132}Te, ^{130}Xe, ^{134}Xe, ^{135}Xe, ^{136}Xe, ^{133}Cs, ^{134}Cs, ^{135}Cs, ^{136}Cs, ^{137}Cs, ^{138}Ba, ^{139}La, ^{140}Ba, ^{141}Ce, ^{143}Ce, ^{144}Ce, ^{145}Ce, ^{146}Nd, ^{148}Nd, ^{150}Nd, ^{147}Nd, ^{147}Sm, ^{148}Sm, ^{149}Sm, ^{150}Sm, ^{151}Sm, ^{152}Sm, ^{154}Sm, ^{153}Eu, ^{154}Eu, ^{155}Eu and, ^{156}Eu. See Figure 2.2.

The probability per fission of directly forming a particular nuclide is known as the fission yield and, since the isotopes produced directly from fission are radioactive and generally short-lived, they transmute to another elements. The predominate mode of fission-product decay is by beta and gamma emission, therefore the decay process doesn't change the mass number of the nuclides [17].

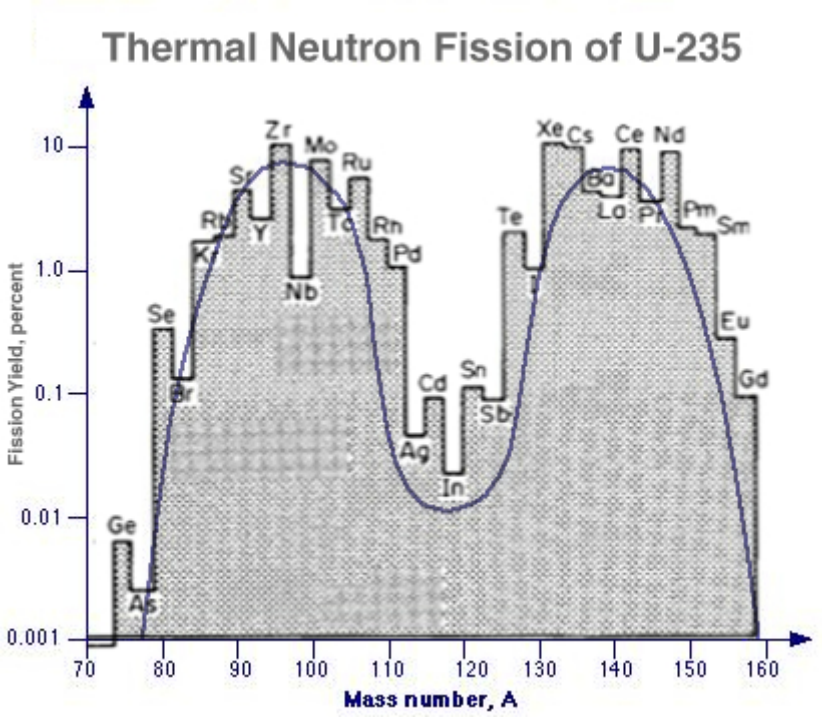

Figure 2.2: Fission-product yields and mass distribution for thermal fission neutrons in $^{235}\mathrm{U}$ [26].

One method for the direct measurement of the fission products is the gamma spectrometry technique. Data such as: characteristic gamma-ray energy, intensity, half-life and yield factor, are needed to correct experimental data in order to be able to perform a comparison with the theoretical expected values. For a list of commonly measured fission products from $^{235}\mathrm{U}$, see Table 2.2.

In Table 2.2, for the fission products that appears in the form X/Y, the X indicates the main nuclide and the Y indicates a short-lived nuclide that is part of the decay chain of X.

Fission products have a large influence on the behavior and mechanical properties of the FEs. These products can affect the thermal performance of the FE by means of affecting the thermal conductivity and the melting point to mention some. The magnitude of the potential problems arising from the introduction of fission products into the fuel depends on the expected concentration of said fission products. Since all the fission products absorb neutrons to some extent, from the elements presented in Figure 2.2, the gases $^{135}\mathrm{Xe}$ and $^{149}\mathrm{Sm}$ are the most noticeable ones because they have the most significant cross section and, when produced, can have a noticeable effect on the neutron balance in thermal reactors [17, 19, 26].

Table 2.2: Short and middle, lived gamma emitters fission-products data for ^{235}U in a thermal neutron flux. Where $T_{1/2}$ is the half-life, E_γ and I_γ are the energy and the emission intensity of the main emitted gamma rays and, Y is the is the average fission yield of the fission product [25, 27].

Fission product	$T_{1/2}$ [days]	E_γ [keV]	I_γ [%]	Y [%]
^{95}Zr	64.032(6)	724.2	44.27(22)	6.50(1)
		756.4	54.38(22)	
		235.7	0.24	
^{97}Zr/^{97m}Nb	0.6980(3)	657.9	98.23(8)	5.99(2)
		743.4	93.09(16)	
^{99}Mo/^{99m}Tc	2.7470(4)	140.5	89.06(24)	6.13(2)
^{103}Ru/^{103}Rh	39.26(2)	497.1	91(1)	3.10(3)
		610.3	5.64	
		557.0	0.832	
^{105}Rh	1.743(2)	318.9	19.1	0.95(1)
^{106}Ru/^{106}Rh	371.8(2)	621.9	9.93	0.3996
		511.9	20.70	
		1050.3	1.50	
^{131}I	8.025(1)	364.5	81.5(8)	2.88(1)
^{132}Te	3.204(13)	228.2	88(3)	4.28(1)
^{134}Cs	752.42	604.7	97.6	6.7031[a]
		795.8	85.4	
		569.3	14.5	
		801.9	8.73	
		563.2	8.38	
^{137}Cs/^{137m}Ba	10 979(33)	661.6	85.10(20)	6.2109
^{140}Ba/^{140}La	12.753(2)	162.7	6.22(9)	6.31(2)
		537.2	24.39(22)	
		1596.5	109.9	
		487.0	52.9	
^{141}Ce	32.508(13)	145.4	48.29(20)	5.86(3)
^{144}Ce/^{144}Pr	284.91(5)	133.5	11.09(19)	5.4824
		696.5	1.34	
		80.1	1.13	
		2185.7	0.70	
^{143}Ce	1.376(2)	293.3	42.8(4)	5.94(2)
^{147}Nd	10.98(1)	91.0	28.1(5)	2.22(2)
		531.0	13(1)	

[a] Obtained from ^{133}Cs (n,γ) ^{134}Cs i.e., ^{133}Cs neutron capture process.

Among the gases produced that will have a direct impact on the mechanical properties are the Kr and Xe gases, including its decay precursor such as iodine. These elements are gaseous at normal conditions. This rejection will cause the formation of bubbles, which in turn will cause the FE to swell or the gases will diffuse to the surface of the fuel and will increase the pressure inside the sealed fuel cladding. Either way is detrimental for the FE performance. Hence fission gas behaviour is a strong determinant of fuel element design and performance [17, 26].

For the particular case of the U-ZrH fuel, the swelling due to fission products is proportional to the burnup and, is ≈ 3 times larger than that of oxide fuels and also, there are experimental results that prove that only a small fraction of the fission products are released even in completely unclad fuel; the release fraction varies from 1.5×10^{-5} for an irradiation temperature of 350 ºC to, $\approx 10^{-2}$ at 800 ºC [28, 29].

2.3 Theoretical Burnup

Theoretical burnup is obtained by means of the concentration of the selected fission product, as well as the proper correction factors.

2.3.1 Concentration, theoretical

The concentration (atoms/cm^3) of a fission product is directly correlated with the FEs burnup. The following non-homogeneous, first-order, ordinary differential equation describes how to find the concentration of a fission product x (i.e., the burnup monitor), due to the ^{235}U fissions during an irradiation time t_i.

$$\frac{dN_x}{dt_i} = \sigma_u^f \phi Y_x N_u - \lambda_x N_x - \sigma_x^c \phi N_x \tag{2.2}$$

where N_x is the concentration of the x fission product, σ_u^f is the fission microscopic cross-section of ^{235}U, ϕ is the neutron flux, Y_x is the yield factor for the fission product x, N_u is the initial concentration of the of ^{235}U atoms, λ_x is the decay constant of the fission product x and, σ_x^c is the capture microscopic cross-section of the fission product x.

From equation (2.2), on the RHS, the first term from left to right, is the creation rate of the fission product x due to the ^{235}U fissions. The following two terms are the loss rate due to radioactive decay and neutron capture of the x fission product, respectively. By

factorizing equation (2.2), it can be rearrange as follows,

$$\frac{dN_x}{dt_i} = \sigma_u^f \phi Y_x N_u - (\lambda_x + \sigma_x^c \phi) N_x \tag{2.3}$$

and establishing,

$$\lambda = \lambda_x + \sigma_x^c \phi \tag{2.4}$$

rewriting equation (2.3), it is obtained

$$\frac{dN_x}{dt_i} = \sigma_u^f \phi Y_x N_u - \lambda N_x \tag{2.5}$$

and regrouping terms is obtained,

$$\frac{dN_x}{dt_i} + \lambda N_x = \sigma_u^f \phi Y_x N_u \tag{2.6}$$

$$dN_x + \lambda N_x dt_i = (\sigma_u^f \phi Y_x N_u) dt_i \tag{2.7}$$

the previous equation is a first order differential equation of the form:

$$Q_{(x)} dx = dy + p_{(x)} \cdot y dx$$

that can be solve my means of the integration factor method. Let it be $p_{(x)} = \lambda$ then the integration factor is,

$$F.I = e^{\int p_{(x)} dx} = e^{\int \lambda dt_i} = e^{\lambda t_i}$$

multiplying both sides of equation (2.7) by the integration factor gives,

$$e^{\lambda t_i} dN_x + e^{\lambda t_i} \lambda N_x dt_i = e^{\lambda t_i} (\sigma_u^f \phi Y_x N_u) dt_i \tag{2.8}$$

and this can be rewritten as,

$$d\left[e^{\lambda t_i} N_x\right] = (\sigma_u^f \phi Y_x N_u) e^{\lambda t_i} dt_i \tag{2.9}$$

integrating both sides

$$\int d\left[e^{\lambda t_i} N_x\right] = \int (\sigma_u^f \phi Y_x N_u) e^{\lambda t_i} dt_i \tag{2.10}$$

$$e^{\lambda t_i} N_x = (\sigma_u^f \phi Y_x N_u) \left[\frac{e^{\lambda t_i}}{\lambda} + C\right] \tag{2.11}$$

$$N_x = (\sigma_u^f \phi Y_x N_u) \left[\frac{1}{\lambda} + C e^{-\lambda t_i}\right] \tag{2.12}$$

at $t = 0$ the fuel is considered fresh, therefore the concentration of any fission product $N_x(0) = 0$, substituting this boundary conditions in the previous equation and solving for C gives,

$$C = \frac{-1}{\lambda} \tag{2.13}$$

substituting the obtained value of C back in equation (2.12), gives the following,

$$N_x = \frac{\sigma_u^f \phi Y_x N_u}{\lambda} \left[1 - e^{-\lambda t_i}\right] \tag{2.14}$$

and finally, substituting equation (2.4) back, into the previous equation yields,

$$N_x(t_i) = \frac{\sigma_u^f \phi Y_x N_u}{\lambda_x + \sigma_x^c \phi} \left[1 - e^{-(\lambda_x + \sigma_x^c \phi) t_i}\right] \tag{2.15}$$

The term outside the brackets is known as *saturation factor* and, the term inside as *burnup and decay decrease factor*.

2.3.2 Corrections factors

In order to achieve the correct values of the concentration of the selected monitor and, therefore be able to compare them with the experimental data, is necessary to compensate the effects produced by decay and burnup of the monitor, and position and power of the FE's on each cycle or irradiation configuration. Due to the previous, the following correction factors are considered:

2.3.2.1 Decay of burnup monitor correction factor

This correction factor considers the decay and burnup of the monitor for different irradiation periods and partial decay times underwent by the FE and is given by [30],

$$f_d = \frac{\lambda_x \sum_{k=1}^{n} P_k \cdot t_k}{\sum_{k=1}^{n} P_k \cdot e^{-\lambda_x \tau_k}\left[1 - e^{-(\lambda_x + \sigma_x^c \phi)t_k}\right]} \tag{2.16}$$

where P_k is the average relative power corresponding to the kth irradiation period (been $\sum_k^n P_k$=1), n is the total number of irradiation periods during the whole irradiation history of the fuel element, t_k is the duration of the kth irradiation period, and τ_k is the time interval between the end of the kth irradiation period and the end of the last irradiation period.

2.3.2.2 Average power correction factor

Since the neutron flux in the core is not homogeneous, it is convenient to consider the *power factor* F_p, defined as the ration between the average neutron flux at the position where the FE was present and the core average neutron flux for the given core configuration. Due to the working loads and different experiments developed at the reactor, the FEs were in different positions during the irradiation time and exposed to different neutron flux and spectra, this correction can be taken into account by introduction of a weighted power factor for the different configurations in which the FEs where irradiated. This factor is known as the average power correction factor, and is given by [12],

$$\overline{F_p} = \sum_{i}^{m} P_i \cdot (F_p)_i \tag{2.17}$$

where $\overline{F_p}$ is the average power correction factor, P_i is the average relative power corresponding to the i-th irradiation position, and m the total amount of positions where the fuel element was present.

The reactor core of a typical TRIGA reactor has a annular configuration. For a Mark TRIGA II reactor, the fuel elements inside the core are arranged in six concentric rings, labeled A, B, C, D, E and F, having 1, 6, 12, 18, 24 and 30 locations, respectively [24], see Figure 4.3.

For a Mark TRIGA III reactor an additional ring labeled G can be found. This ring is

filled with graphite elements which are used as reflectors [12], see Figure A.1.

2.3.3 Activity, theoretical

From the concentration and the correction factors, the theoretical activity of the selected fission product can be estimated,

$$A_T = \lambda_x N_x V_{fe} \left(e^{-\lambda_x t_d}\right) f_d \overline{F_p} \tag{2.18}$$

where V_{fe} is active fuel volume from the FE and, t_d is the cooling-down time outside of the reactor core.

2.3.4 Burnup equation, theoretical

The fissioned mass of $^{235}\mathrm{U}$ in the irradiated fuel element is given by [30],

$$m_u = \frac{(N_x V_{fe})}{Y_x} \frac{m_u^0}{N_u^0} \tag{2.19}$$

where m_u is the $^{235}\mathrm{U}$ consumed mass, m_u^0 is the initial mass and, N_u^0 is the initial number of atoms of $^{235}\mathrm{U}$ isotope in the FE. From the relation $m_u^0/N_u^0 = M_u/N_A$, where M_u is the atomic weight of $^{235}\mathrm{U}$ and N_A is Avogadro number, the previous equation becomes,

$$m_u = \frac{(N_x V_{fe})}{Y_x} \frac{M_u}{N_A} \tag{2.20}$$

The fissile nuclides are consumed by means of fission and capture, hence the total probability of this two events to happened is defined as $(1+\alpha)$, where α is the *capture-to-fission ratio* defined as [14],

$$\sigma_c/\sigma_f = \alpha \tag{2.21}$$

Therefore, by also applying the correction factors, from Section 2.3.2, the burnup equation is

$$B_T = \frac{(N_x V_{fe})}{Y_x} \frac{M_u}{N_A} (1+\alpha) \cdot f_d \cdot \overline{F_p} \tag{2.22}$$

For the particular case of the $^{235}\mathrm{U}$, the thermal value for α = 0.17. The burnup has units of mass (g).

Chapter 3

Fuel burnup determination methods

Accurate fuel burnup analyses are essential for research purposes, reactor operation, determination of fuel cycle costs and, providing experimental data that is a prerequisite for validating computer codes. The main methods to experimentally determine fuel burnup on FEs are described. Destructive and non-destructive methods have been used and studied extensively. Among the destructive methods, mass spectrometry and radiochemical assay can be found. For the non-destructive methods reactor physics calculations, reactivity measurements and, γ-ray spectrometry can be found [31, 32].

3.1 Destructive methods

Without detailed knowledge of the initial fuel loading, the most accurate methods for determining burnup are chemical-based analyses which rely on the determination of specific nuclides after appropriate separation procedures for the determination of actinides and fission products. This techniques in particular are considered expensive, time consuming and therefore, are not normally performed by the reactor operators [31, 32, 33].

Destructive methods can be classified into two methods depending on the considered elements that are being analyzed [33]:

- Based on the determination of the heavy element depletion before and after irradiation.
- By determining the amount produced of a selected fission product. For this analysis it must suffice the following characteristics:

- Same fission yield for all fissioning isotopes of interest,
- not be present as an impurity,
- not be formed during irradiation by another process,
- have a small absorption cross-section for neutron capture,
- have precursors with short half-life and/or small or negligible absorption cross-section,
- have no gaseous precursors,
- be easily chemically separated from the fuel matrix,
- be readily determined by an accurate chemical-analytical procedure.

3.1.1 Mass spectrometry

Burnup can be calculated by using the measured mass of a specific fission product in the fuel, the cumulative fission yield of that specific fission product, and the total mass of actinides present in the sample. Ideally, the fission products used in the calculations should have a small neutron absorption cross section, a high cumulative fission yield and, chemically the fission product must also readily dissolve during the leaching process. This technique uses the following formula to calculate burnup [34],

$$BU_{\%} = 100 \cdot \frac{(N_{fp}/Y_{fp})}{(N_{fp}/Y_{fp}) + N_{act}} \tag{3.1}$$

where $BU_{\%}$ is the burnup given in %, N_{fp} is the number of atoms of a specific fission product measured in the sample, Y_{fp} is the cumulative fission yield of the fission product and, N_{act} is the number of atoms of actinides in the sample.

There are six isotopes that work for mass spectrometry analysis of the fuel: $^{139}\mathrm{La}$, $^{140}\mathrm{Ce}$, $^{142}\mathrm{Ce}$, $^{141}\mathrm{Pr}$, $^{145}\mathrm{Nd}$, $^{146}\mathrm{Nd}$. These isotopes occur on the higher atomic number peak of the binomial fission product distribution and are nonradioactive and have relatively small neutron absorption cross section with the exception of Nd-145. Because of its cross section, the number of Nd-145 and Nd-146 atoms in the samples and their respective yields are summed in the calculation of burnup [32, 34].

3.1.2 Radiochemical assay

Destructive radiochemical analysis of spent nuclear fuels is an important tool to determine burnup with high accuracy and to better understand the formation process of actinides and fission products during irradiation as a result of fission and successive neutron capture. The data bases and isotope inventories resulting from the analysis, are of high importance to evaluate the performance of nuclear fuels in a reactor, to validate computer codes applied for a safe transport, storage and disposal/reprocessing of spent fuels and to safeguard fissile material [35, 36].

In radiochemistry burnup is expressed as %FIMA, i.e. the number of fissions that have occurred per Initial 100 heavy Metal Atoms (U and/or Pu). The number of fissions that occurred during irradiation can be derived from the concentration of selected key fission products in the spent fuel sample under analysis. The accurate detailed radiochemical analysis of irradiated fuel requires a well-designed analysis scheme incorporating appropriate separations, measurements and cross-checks of the samples [36].

3.2 Non-destructive methods

The capability to assay fuel assembles without destroying them is of vital importance in view of: the operational efficiency and safety needed for the nuclear fuel cycle and, an effective international safeguards since this techniques can provide fissile inventory on irradiated fuel either stored or shipped or, to be reprocessed [37].

3.2.1 Reactor physics calculations

More common in practice than the experimental methods, described later, particularly when dealing with a large number of FEs , due to its practicality for routinely updates. From late 1980s, the arduous task of solving the neutron transport equations was relegated to computers, with a varying degree of approximations to be able to deal with the different materials comprising the reactor, the constant changes in the fuel composition and, the complex energy dependence of the microscopic neutron cross-section over the energy spectrum found in a nuclear reactor [1, 31, 37].

Nowadays these computer codes have evolved from a simple aid to become a standard part of the research and development programs and, are capable to perform routinely reactor calculations such as [1]:

- detailed burnup determination,
- core design and fuel management,
- core optimization for production of particular isotopes,
- power distribution analysis of mixed cores,
- design of experiments,
- safety analyses and,
- excess reactivity and shutdown margin.

The burnup calculations are based on two main equations in reactor physics: the burnup equations, see Section 2.3, and the neutron transport equation. The later, been basically an equilibrium equation for neutron density, that would give as a solution a neutron density distribution that will allow to compute the rates at which the elements are transforming inside the FE [38].

In Slovenia the TRIGLAV code was developed to calculate burnup in TRIGA fuel. It is based on neutronic diffusion code for TRIGA reactor calculations. The program is based on 4-group time independent homogeneous diffusion equation in a two-dimensional cylindrical geometry. The equation for an energy group g is given [1],

$$-\nabla D^g \nabla \Phi^g + \Sigma_r^g \Phi^g = \left(\frac{1}{k}\right) \chi^g F + \sum_{g'=1, g' \neq g}^{4} \Sigma^{g' \to g} \Phi^{g'}; \quad g = 1, ..., 4 \tag{3.2}$$

$$\Sigma_r^g = \Sigma_r^a + \sum_{g'=1, g' \neq g}^{4} \Sigma^{g' \to g} + D^g B_z^2 \tag{3.3}$$

$$F = \sum_{g=1}^{4} \nu^g \Sigma_f^g \Phi^g \tag{3.4}$$

where Φ^g is the neutron flux, D^g is the diffusion constant, Σ_r^g is the removal cross-section, B_z is the axial geometrical buckling, $\Sigma^{g' \to g}$ is the scattering cross-section from group g' to group g, χ^g is part of the fission spectrum in group g, k is the multiplication factor, F is the fission density that is compose by, ν^g as the number of fission neutrons in the energy group g and, Σ_f^g is the fission cross-section for group g. The diffusion equation is solved by the finite difference method.

3.2.2 Reactivity measurements

In comparison with the previously described methods, it is consider a relatively simple one, to determine the burnup of either a single FE or from whole assemblies, since the only quantity measured is the excess reactivity from the reactor core. However, this methodology can only provide relative differences between the FEs burnups, therefore a reference measurement is needed. It needs to be combined with another methods in order to obtain absolute burnup values. Three variants of the methodology can be considered [31, 39]:

- The analytic reactivity method. Nowadays, involves the use of computer codes to estimate the neutron flux and the multiplication factor, but is always necessary to obtain a reference burnup value.
- The linear reactivity method. Assumes that the relation between the multiplication factor and the burnup is approximately linear, can be given by [39],

$$\Delta k \approx BU_i - BU_0 \tag{3.5}$$

  where Δk is the difference between the multiplication factors, Bu_i is the burnup of the i measure and, Bu_0 is the burnup reference measure.
- polynomial method. Similar to the linear method but a low order polynomial function with a short exponential contribution due to poison build-up is assumed, a function of the form is then used [40],

$$\Delta k(BU) \approx a + b \cdot BU + c \cdot e^{-d \cdot BU} \tag{3.6}$$

  where a, b, c and d, are fitting parameters.

3.2.3 Gamma-ray spectrometry

This method measures the activity of very carefully selected fission product that is proportional to the burnup, but also has very important characteristics related to the half-life, fission yield and, neutron capture cross-section. The methodology requires a precise experimental arrangement for the scanning of the FEs , as well as a calibrated high resolution detector. This technique has advantages, disadvantages and a particular methodology that would be explained in detail on the following section.

Chapter 4

Gamma spectrometry

From all the possible methods mentioned before, the γ-ray spectrometry non-destructive assay (NDA) has been the most common from the experimental point of view, since can be applied without the need for detailed data on FEs irradiation history [31, 41].

4.1 Advantages and disadvantages

In relation to the other methods presented before gamma spectrometry present the following advantages [27]:

- It is a non-destructive method, so the irradiated nuclear fuel remains intact during measurements, preventing the release of fission products;
- In relation to chemical methods for burnup determination, it is considered more accurate and faster, in addition to not requiring the destruction of spent nuclear fuel;
- Allows the determination of the number of fissile nuclei remaining in the spent FE and the calculation of the decrease in the $^{235}\mathrm{U}$ and $^{238}\mathrm{U}$ quantities in it, even allowing to evaluate the convenience of returning the examined nuclear fuel to the reactor core;
- It has a low cost of use as long as you already have the equipment necessary;

And the disadvantages presented in said method are [27, 39]:

- Can present a significant error associated with difficulties in measuring the absolute

efficiency of the experimental apparatus to be used;

- It requires detailed and accurate records of the time and radiation power to which the FE to be examined was subjected;
- The background radiation must be as low as possible, so that it does not interfere with the results of the measurements.
- Involve some operational inconveniences like the cool-down time and the handling of the FE outside the reactor pool.

4.2 Burnup monitor

For the gamma spectrometry method, the measurement of specific fission products is necessary, this nuclides are called monitors. An ideal monitor for a FE is the one that has the following characteristics [12, 27]:

- In each fission suffered by a heavy core, the monitor must be produced in an approximately constant amount, so that the monitor's production is proportional to the burnup level.
- Must have a long half-life in relation to the total irradiation time, so that the proportionality between the particles emitted by the monitor and the number of fissions become valid, i.e., must be consistent during a reasonable period of time.
- Must have low migration along the fuel because if the monitor and its precursors were not consistent, they will suffer a displacement in relation to their formation positions and, consequently, the determined burning value will end up suffering distortions, i.e., must be as consistent as possible in the position along the FEs.
- The spectrum emitted must contain high-energy gamma rays, which reduces the attenuation effects to which they are subject when they emerge from the irradiated nuclear fuel, i.e., must decrease the self-attenuation effects of the FEs.

Therefore the fission products from Table 2.2, with *half-lifes*[1] longer than 10 days and energies above ≈500 keV, to avoid the Compton continuum, can be considered for the use of burnup monitors.

[1] Expectation value of the time required for one-half of the initial number of nuclei to disintegrate, and hence for the activity to decrease by half [42].

The ^{137}Cs, is the burn monitor par excellence. Has a relatively long half-life, a low absorption neutron cross-section of (0.27±0.03) b and, it formation is proportional to ^{235}U. A remark regarding the use of ^{137}Cs as a monitor, is the suggested waiting time of approximately two years to avoid overlap of the characteristic photo-peak with the short-lived elements with higher intensity [27, 31].

Since ^{134}Cs is the result for the neutron capture process from ^{133}Cs nuclide, to use ^{134}Cs as a burnup monitor a detailed knowledge of the neutron flux is required during the irradiation time and also the capture cross-section for the thermal neutrons energy of 0.025 eV, and it can only be seen after a cooling down period of 1-2 months [31].

And for ^{144}Ce/ ^{144}Pr, ^{140}Ba/ ^{140}La, ^{103}Ru/ ^{103}Rh and, ^{95}Zr, that are the rest of the nuclides with a relatively high half-life (longer than 10 days) and have energies above the 500 keV with relatively high intensities, are recommended for the low irradiation and low cooling periods. A worthy remark for the ^{144}Ce/ ^{144}Pr, is the low intensity for the high energy photon that produce.

For the reasons stated above, the following nuclides can be consider as burnup monitors, see Table 4.1.

Table 4.1: Main properties of fission products used as monitors of ^{235}U burnup from irradiated FEs for the gamma spectrometry technique. Where $T_{1/2}$ is the half-life, E_γ and I_γ are the energy and the emission intensity of the main emitted gamma rays and, Y is the is the average fission yield of the burnup monitor for ^{235}U [12, 30].

FE history		Burnup	$T_{1/2}$	E_γ	I_γ	Y
Irradiation	Cooling	monitor		[keV]	[%]	[%]
$<$ 40 d	$>$ 9 d	^{140}Ba/ ^{140}La	12.75 d	1596.5	109.9	6.18(13)
$<$ 200 d	$>$ 40 d	^{95}Zr	64.03 d	724.2 756.7	43.7 55.4	6.41(9)
$\leq$ 1000 d	$<$ 2 yr	^{144}Ce/ ^{144}Pr	284.9 d	2185.7	0.7	5.34(16)
$>$ 1800 d	$\geq$ 2 yr	^{137}Cs/^{137m}Ba	30.15 yr	661.66	85.1	6.26(4)

4.3 Detector coefficients

During measurements, gamma-ray detection is performed with an High-Purity Germanium (HPGe) detector in conjunction with associated electronic modules. In order to be able to take valid measurements with said equipment, a series of calibration coefficients should be applied.

4.3.1 Energy calibration coefficient

The gamma spectra resulting from the measurements of the irradiated FE will show the number of counts in the photopeaks as a function of the channels they occupy, providing direct information on what is the gamma-ray energy that gave rise to a particular photopeak in the spectrum obtained. Nevertheless, before measuring on the FE, the energy calibration as a function of the channel number is required in order to identify in each gamma spectrum, the photopeaks corresponding to the gamma rays emitted in the decay of the burnup monitors and, this relationship between the channel number and photopeak energy should be of linear nature. See Section 5.1 for more detail.

4.3.2 Detector efficiency calibration coefficient

After the localization and identification of the corresponding gamma-ray photopeak for the selected monitor, it becomes necessary to determine the absolute efficiency by means of the intrinsic efficiency of the detector and the solid angle subtended, due to the collimation, from the emitting source to the detector. See Section 5.2 for more detail.

4.4 TRIGA Mark II reactor

The JSI TRIGA Mark II reactor has been operating since 1966. It is being utilized as a training facility for reactor operators, medical isotope production facility and for the execution of different reactor physics experiments. It is a pool type light-water thermal research reactor, with a maximum power of 250 kW and a maximum neutron flux of approximately 10^{13} neutrons/cm^2-s [24], see Figure 4.1 and Figure 4.2.

The reactor core has a cylindrical configuration and is composed of cylindrical fuel rods clad with stainless steel. The core of the TRIGA reactor is located at the bottom of the reactor tank, approximately 5.30 m from the platform bridge. The reactor pool is filled with purified water and has the shape of an aluminum cylinder with a height of 6.25 m and 2 m diameter. The core itself has a cylindrical configuration and is in general composed of fuel elements and two aluminum supporting grids. Holes are drilled in both supporting grids that enable the insertion of fuel elements, control rods, irradiation channels and neutron source – these holes have a diameter of 3.8 cm. Beside the larger holes also smaller ones, with a diameter of 10.5 mm or 8 mm, are drilled in the grids. These are intended for the insertion of specially adapted instrumentation guides that enable the use of neutron

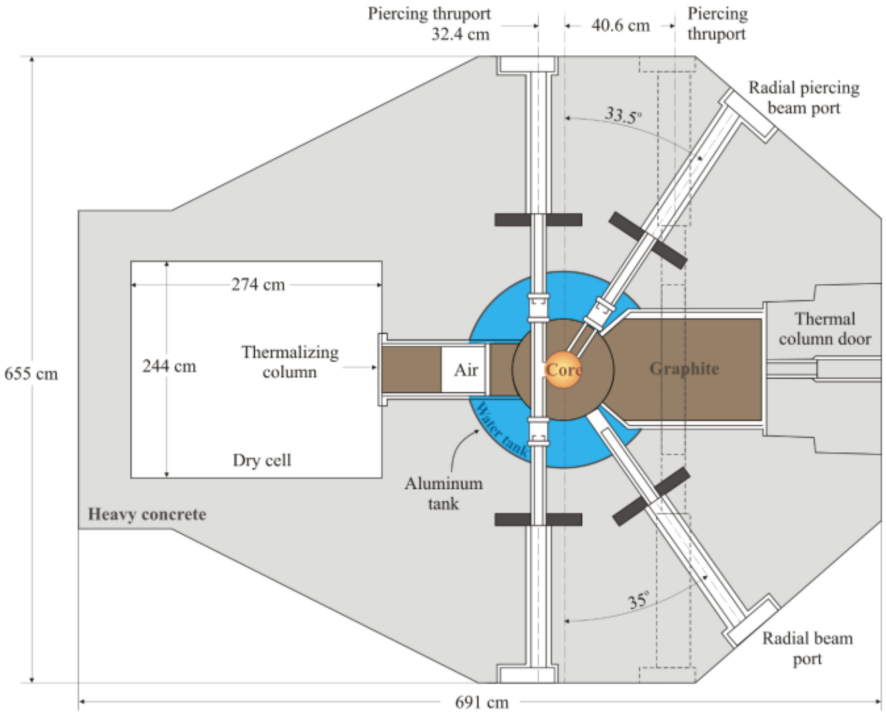

Figure 4.1: Top view of the IJS TRIGA Mark II reactor [24].

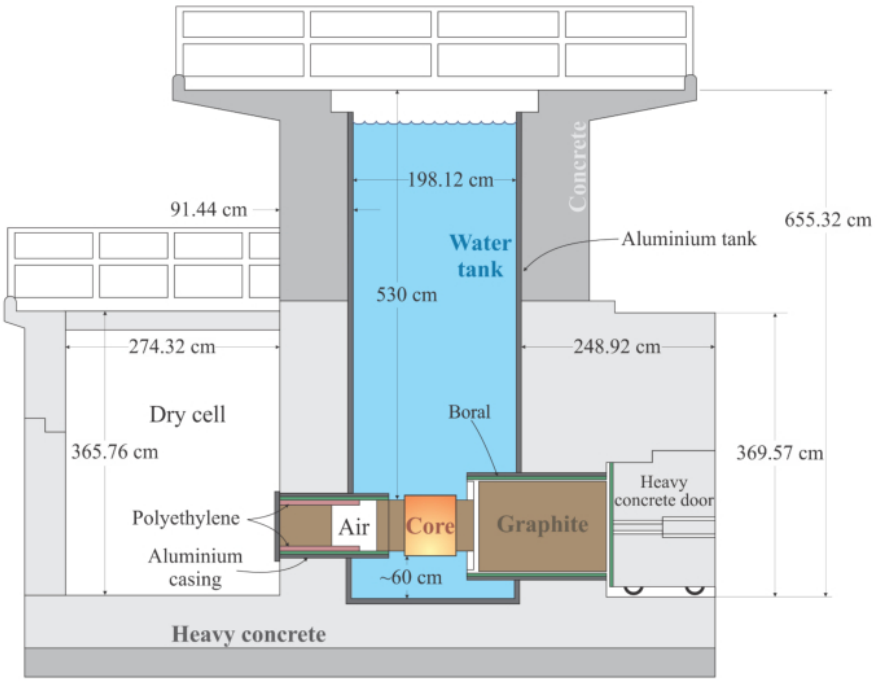

Figure 4.2: Side view of the IJS TRIGA Mark II reactor [24].

detectors inside the core of the TRIGA reactor. Two larger triangular holes are utilized for the insertion of either three fuel elements or a triangular irradiation channel [24], see Figure 4.3.

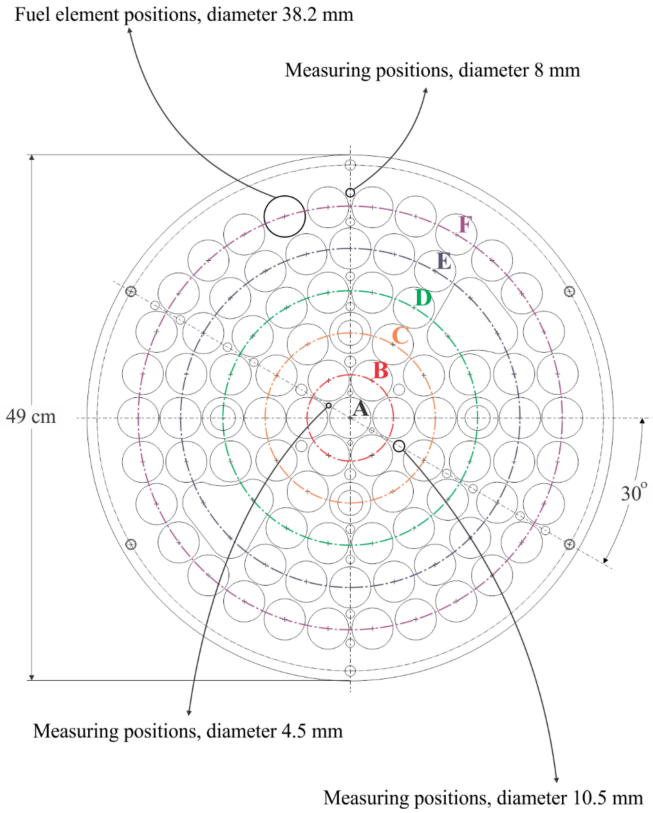

Figure 4.3: Schematic view of the core positioning ring at the IJS TRIGA Mark II reactor [24].

4.5 Experimental Burnup

A critical part for the experimental burnup determination is the experimental arrangement for the gamma scanning of the FE. Typically this kind of experiments are developed in the reactor pool [24, 27, 30, 43] or in the spend-fuel storage pool [31, 44, 45, 46] and therefore, using the water as shielding for radiation protection purposes, see Figure 4.4c.

Usually the spent fuel is positioned several meters under water with a scanning device on top of the pool, see Figure 4.4c. It is therefore very important that the position of the scanning device can be reproduced accurately [31, 45].

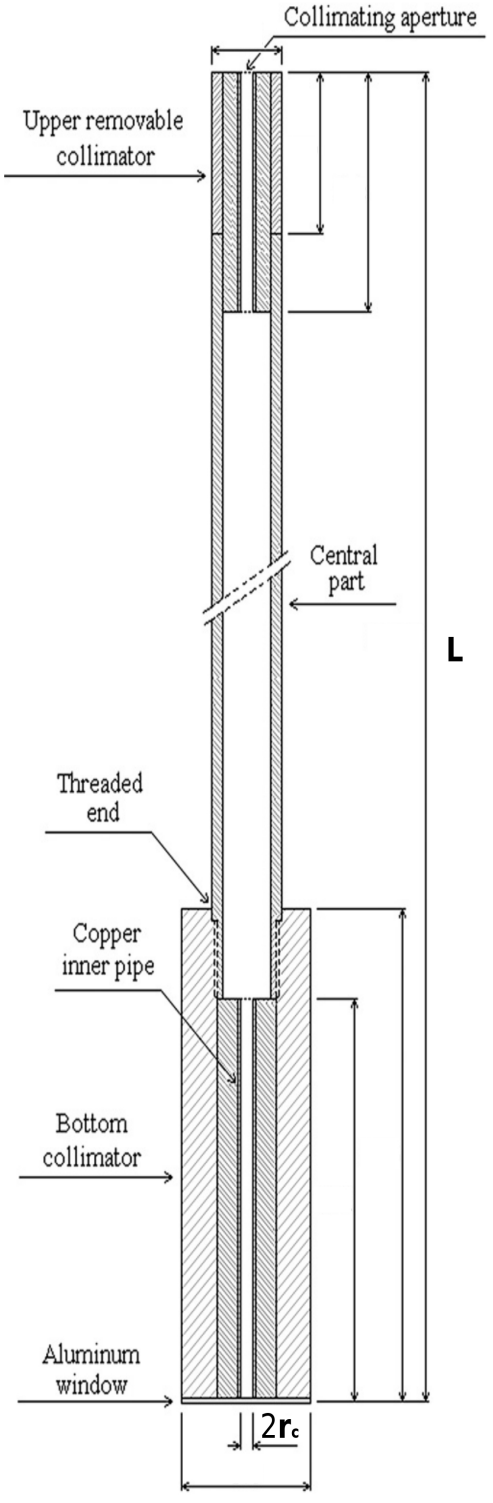

(a) Cross-sectional diagram of a collimator tube [46].

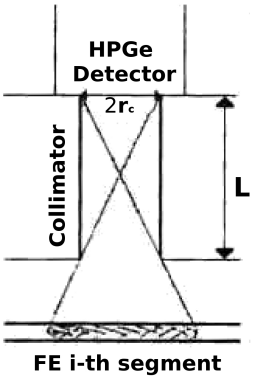

(b) Simplified geometry for the i-th measurement over the FE [27].

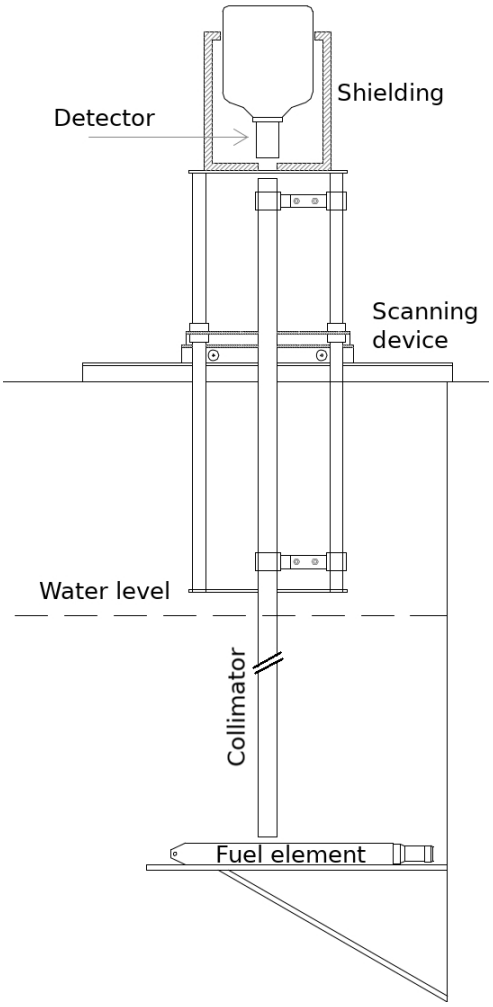

(c) Experimental setup for scanning of a fuel element inside a pool [45].

Figure 4.4: Schematic representation, by parts, of the experimental setup for the gamma spectroscopic measurement.

An important characteristic of any experimental setup involving gamma-rays measurements is obtaining the narrow-beam attenuation for primary particles and therefore, the narrow-beam geometry. The primary beam will be comprised by the particles that are perpendicularity reaching the detector, i.e., at an angle $\approx 0^{o}$. The secondary particles can be considered, in broad terms, as the decay and scatter particles from the primary beam.

In order to achieve the narrow beam attenuation, detector shielding, filtering and, collimation of the gamma-rays, see Figure 4.4a, are used. Both with the intention of preventing the secondary particles from reaching the detector and to achieve a narrow-beam geometry.

An air-filled collimator tubes typically have a length of several meters. In addition, lead plugs with about 5 mm collimator diameter can be inserted into the collimator tube, see Figure 4.4a. Shielding the detector helps to increase the resolution and to reduce the detector dead time [31].

4.5.1 Correction factors

Because it is intended to perform gamma-ray measurements, correction factors should be applied. Among the main correction factors to take into account are the ones due to the gamma-rays attenuation on different stages before reaching the detector, detector related coefficients and, the *decay of burnup monitor correction factor* (f_d), see Section 2.3.2.1.

4.5.1.1 Self-attenuation coefficient

The self-attenuation coefficient, considers the reduction of the gamma-rays counts due to the homogeneous mixture of the fuel composition. It is assumed that the FE is a uniform cylinder with height h and radius R_o, which in its center has a stable Zr bar of radius R_i. See Figure 4.5.

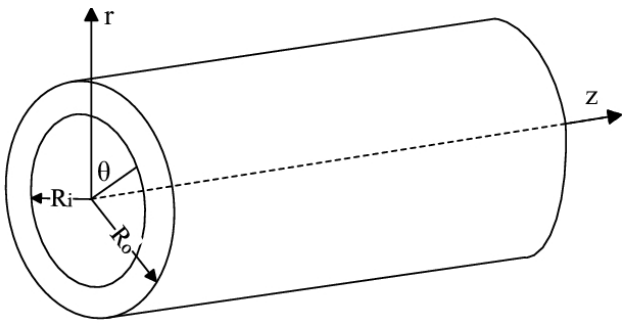

Figure 4.5: Fuel element representation in cylindrical coordinates.

Since the FE is an homogeneous volumetric source, a constant "gamma-emitting density" ρ_γ given in (γ/cm^3-s), can be defined. Therefore, the intensity, considering the attenuation, due to the whole FE is given by,

$$I = \int_{R_i}^{R_o} \int_0^{2\pi} \int_0^h \left(\rho_\gamma \cdot e^{-\mu(R_0 - r)}\right) r dr d\theta dz \tag{4.1}$$

where μ is the attenuation coefficient. This can be further refine by considering the stainless steel (SS-304) cladding with a thickness D_s and an attenuation coefficient μ_{ss}, this gives

$$I = \int_{R_i}^{R_o} \int_0^{2\pi} \int_0^h e^{-\mu_{ss} \cdot D_s} \left(\rho_\gamma \cdot e^{-\mu(R_0 - r)}\right) r dr d\theta dz \tag{4.2}$$

Now let's consider the intensity without considering any of the attenuation factors,

$$I_0 = \int_{R_i}^{R_o} \int_0^{2\pi} \int_0^h \rho_\gamma \cdot r dr d\theta dz \tag{4.3}$$

Therefore the compensation needed, due to the losses generated due to the fuel mixture attenuation and the SS-304 cladding, would be given by the ratio between equation (4.3) and equation (4.2). This gives,

$$\frac{I_0}{I} = \frac{\int_{R_i}^{R_o} \int_0^{2\pi} \int_0^h \rho_\gamma \cdot r dr d\theta dz}{\int_{R_i}^{R_o} \int_0^{2\pi} \int_0^h e^{-\mu_{ss} \cdot D_s} \left(\rho_\gamma \cdot e^{-\mu(R_0 - r)}\right) r dr d\theta dz} \tag{4.4}$$

$$\frac{I_0}{I} = \frac{\int_{R_i}^{R_o} r dr}{e^{-\mu_{ss} \cdot D_s} \int_{R_i}^{R_o} e^{-\mu(R_0 - r)} r dr} \tag{4.5}$$

after solving the integrals, the previous equation becomes,

$$\frac{I_0}{I} = \frac{\frac{R_o^2 - R_i^2}{2}}{e^{-\mu_{ss} \cdot D_s} \left[\frac{(\mu R_o - 1) - (\mu R_i - 1) \cdot e^{-\mu(R_o - R_i)}}{\mu^2}\right]} \tag{4.6}$$

after simplifying and re-arranging, I_0 becomes,

$$I_0 = I \left[\frac{\mu^2 (R_o^2 - R_i^2) e^{\mu_{ss} \cdot D_s}}{2[(\mu R_o - 1) - (\mu R_i - 1) \cdot e^{-\mu(R_o - R_i)}]}\right] \tag{4.7}$$

taking the attenuation coefficient μ, as the FE attenuation coefficient μ_{fe} then, the value

inside bracket is known as the *self-attenuation coefficient* f_a, given by

$$f_a = \frac{\mu_{fe}^2(R_o^2 - R_i^2)e^{\mu_{ss}\cdot D_s}}{2[(\mu_{fe}R_o - 1) - (\mu_{fe}R_i - 1)\cdot e^{-\mu_{fe}(R_o - R_i)}]} \tag{4.8}$$

Due to the energy dependence of the attenuation coefficients, energy dependent functions for the U-ZrH compound and the SS-304 were developed.

For the U-ZrH compound: using data from reference [47], and the FE nuclide composition from Table 2.1, the following function was developed,

$$\mu_{fe}(E) = 0.2104 + 1.498\cdot e^{\left(\frac{-E}{0.2189}\right)} + 0.4155\cdot e^{\left(\frac{-E}{0.9610}\right)} \tag{4.9}$$

where μ_{fe} is the FE total attenuation coefficient given in cm^{-1} and E is the photon energy given in MeV. The equation is valid in the range, from 0.500 MeV to 5.00 MeV, with a maximum and minimum relative intrinsic error with respect to the data from the reference of 0.59% and -1.20% respectively, see Figure 4.6.

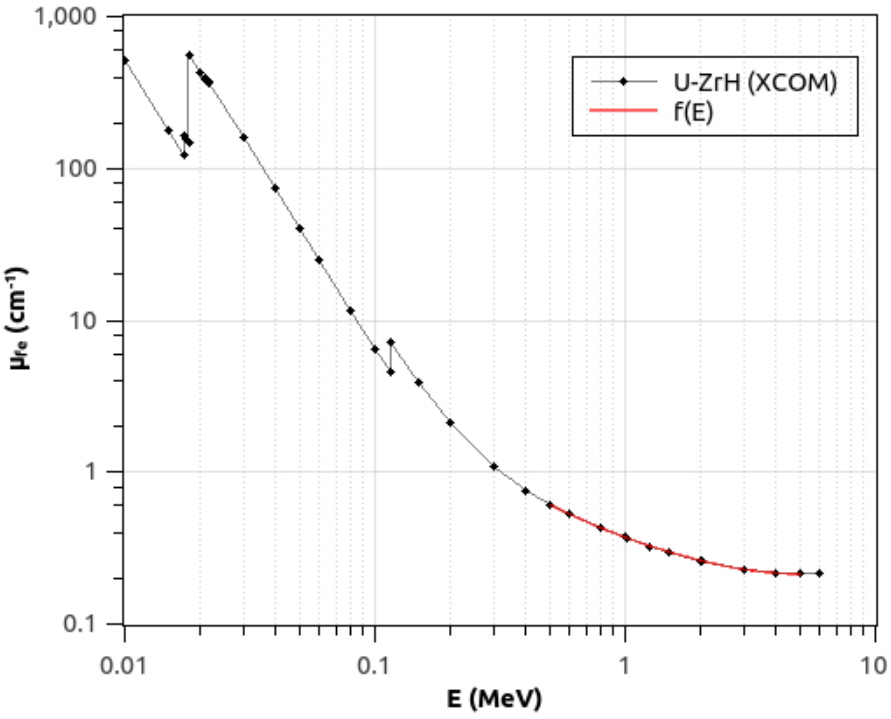

Figure 4.6: U-ZrH compound total attenuation coefficient comparison between the reference [47] and equation (4.9), for the range from 0.500 MeV to 5.00 MeV, with a maximum and minimum relative intrinsic error with respect to the data from the reference, of 0.59% and -1.20% respectively. See Listing C.1, for the fitting results.

For the SS-304 alloy: using data from reference [47], and the FE nuclide composition from Table 2.1, the following function was developed,

$$\mu_{SS}(E) = 0.2368 + 0.4146 \cdot e^{\left(\frac{-E}{1.392}\right)} + 0.5533 \cdot e^{\left(\frac{-E}{0.3584}\right)} \tag{4.10}$$

where μ_{SS} is the SS-304 total attenuation coefficient given in cm^{-1} and E is the photon energy given in MeV. The equation is valid in the range, from 0.500 MeV to 5.00 MeV, with a maximum and minimum relative intrinsic error with respect to the data from the reference of: 0.26% and -0.29% respectively, see Figure 4.7.

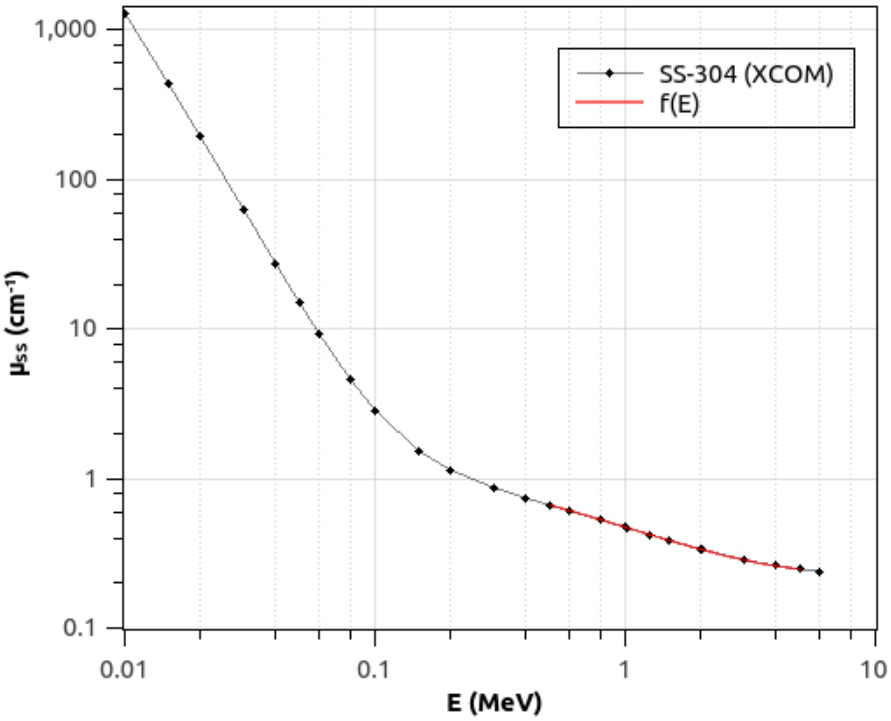

Figure 4.7: SS-304 alloy total attenuation coefficient comparison between the reference [47] and equation (4.10), for the range from 0.500 MeV to 5.00 MeV, with a maximum and minimum relative intrinsic error with respect to the data from the reference of 0.26% and -0.29% respectively. See Listing C.2, for the fitting results.

Since the dimensions of the FE are known from Section 2.2 and the energy of the characteristic photon for the selected burnup monitors are known from Table 4.1, therefore by using equations (4.9), (4.10) and (4.8), the following attenuation coefficients and self-attenuation coefficients were obtained, see Table 4.2.

Table 4.2: Total attenuation coefficients for the U-ZrH nuclide composition and SS-304 alloy, and self-attenuation coefficients for the energies of the burnup monitors from Table 4.1.

E [keV]	$(\mu_{fe} \pm 1.20\%)$ $[cm^{-1}]$	$(\mu_{SS} \pm 0.29\%)$ $[cm^{-1}]$	f_a
661.6	0.4921	0.5820	1.342(5)
724.2	0.4608	0.5566	1.319(5)
756.7	0.4467	0.5445	1.310(4)
1596.5	0.2903	0.3749	1.196(3)
2185.7	0.2532	0.3243	1.170(2)

4.5.1.2 Environmental attenuation coefficient

Before reaching the detector, the gamma rays must pass through a length of water L_w, the thickness of the bottom cap of the collimator tube L_b and, the atmospheric air that fills the entire length L of the collimator tube. This gives rise to an extra correction factor due to environmental conditions, see Figure 4.8.

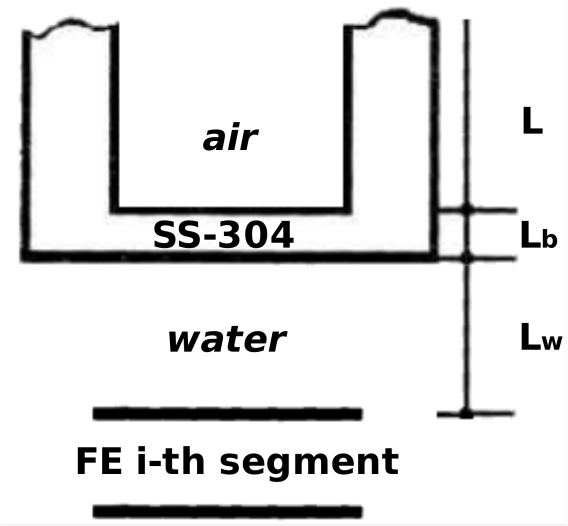

Figure 4.8: Schematic view of the submerged fuel element for the estimation of environmental attenuation coefficients.

Energy dependent functions for dry-air near sea level and water, were developed using data from reference [47], for the burnup monitors energies from Table 4.1.

$$\mu_a(E) = (4.1834 \times 10^{-5}) + (1.1631 \times 10^{-4}) \cdot e^{\left(\frac{-E}{0.9356}\right)} \tag{4.11}$$

$$\mu_w(E) = (3.6826 \times 10^{-2}) + 0.1011 \cdot e^{\left(\frac{-E}{0.9287}\right)} \tag{4.12}$$

where E is the photon energy given in MeV, μ_a is the total attenuation coefficient of dry-air near sea level and, μ_w is the total attenuation coefficient of water, both given in cm^{-1}. The equations are valid in the range, from 0.500 MeV to 3.00 MeV, both with a relative intrinsic error with respect to the data from the reference of $\pm 2.0\%$. Therefore, the environmental attenuation coefficient is defined as,

$$f_v(E; L, L_w, L_b) = exp(-\mu_a(E) \cdot L - \mu_w(E) \cdot L_w - \mu_{ss}(E) \cdot L_b) \tag{4.13}$$

where E is the energy given in MeV. The attenuation coefficients at the gamma energies of the burnup monitors, can be found on Table 4.2 and Table 4.3.

Table 4.3: Total attenuation coefficients for dry-air at sea level and water, for the energies of the burnup monitors from Table 4.1. Both with an estimated error of $\pm 2.0\%$.

E [keV]	$\mu_a \times 10^{-5}$ $[cm^{-1}]$	$\mu_w \times 10^{-3}$ $[cm^{-1}]$
661.6	9.918	8.643
724.2	9.547	8.319
756.7	9.364	8.160
1596.5	6.295	5.495
2185.7	5.308	5.644

4.5.2 Activity, experimental

By means of the gamma spectrometry it is possible to measure the characteristic gamma energies emitted by the selected burnup monitor in the FE; i.e., to determine the experimental activity A_E for the x fission product, which is a direct indicator of the fission in the irradiated fuel.

By considering the necessary correction factors the experimental activity is determined from the total counts from the differential pulse height distribution along the active volume of the FE. The experimental activity is given by [12],

$$A_E = \frac{a}{\epsilon_{ea} \cdot I_\gamma} f_d f_a f_v \tag{4.14}$$

where ϵ_{ea} is the experimental absolute efficiency from the detector. For the case of the FE

analysis, a is defined as

$$a = \sum_{i=1}^{q} \frac{C_i}{t_{c,i}} \tag{4.15}$$

where q is the total amount of measurement done over the active volume of the FE, C_i is the net counts for the i-th measurement, see Figure 4.4b, and $t_{c,i}$ is the total acquisition time for the measurement C_i.

4.5.3 Concentration, experimental

Similarly as in the theoretical concentration calculation, the idea is to find the number of atoms for the selected burnup monitor. At the moment of the measurements the experimental concentration is defined as

$$N_{x,e} = \frac{A_E}{\lambda_x V_{fe}} \tag{4.16}$$

where $N_{x,e}$ is the experimental concentration of the selected burnup monitor given in (atoms/cm^3). Nevertheless, to make possible the comparison between the theoretical and experimental concentrations is necessary to correct for the cooling-down time T_d, of the FE,

$$N_{x,e} = \frac{A_E \cdot e^{\lambda_x t_d}}{\lambda_x V_{fe}} \tag{4.17}$$

4.5.4 Experimental burnup equation

Following the same approach as in Section 2.3.4, the experimental burnup equation for the burnup monitor is,

$$B_E = \frac{(N_{x,e} V_{fe})}{Y_x} \frac{M_u}{N_A} (1 + \alpha) \tag{4.18}$$

where B_E is the experimental burnup given in (g) of the selected burnup monitor.

4.5.5 Possible sources of experimental uncertainty

In any given experiment sources of error exist. In order to avoid or minimize such errors, the possible more significant ones for the previous proposed experiment are presented

below:

- Geometry related sources of error:
  - Collimation errors. This could originate while sweeping the FE. The possible cause: problems in the reproducibility i.e., precision of the positioning system, such as the one presented in Figure 4.4c, specially while moving the scanning device along the FE, therefore it is recommended that the movement of the scanning device be performed in a slow but steady way.
  - Source-detector distance. This could originate from the FE positioning device, during the change of FEs or due to the movement of the scanning device. It is recommended that the FE positioning device and the scanning device could be coupled and therefore allowing to keep a fixed distance.
- Spectrum acquisition related sources error:
  - Unwanted elements appearing on the spectrum. This could originate due to inadequate shielding of the detector.
  - High *dead-time*[2] due to the high activity from the FEs . It is recommended to reduce the collimator radius in order to reduce the number of counts, all of this considering the geometry and the factors associated to it.

4.5.6 Experimental burnup determination flowchart

A simple flowchart representing the steps mentioned in the previous sections, with a suggested workflow, is presented on Figure 4.9.

[2] minimum time of separation between two successive events for proper detection, also called resolving time [8].

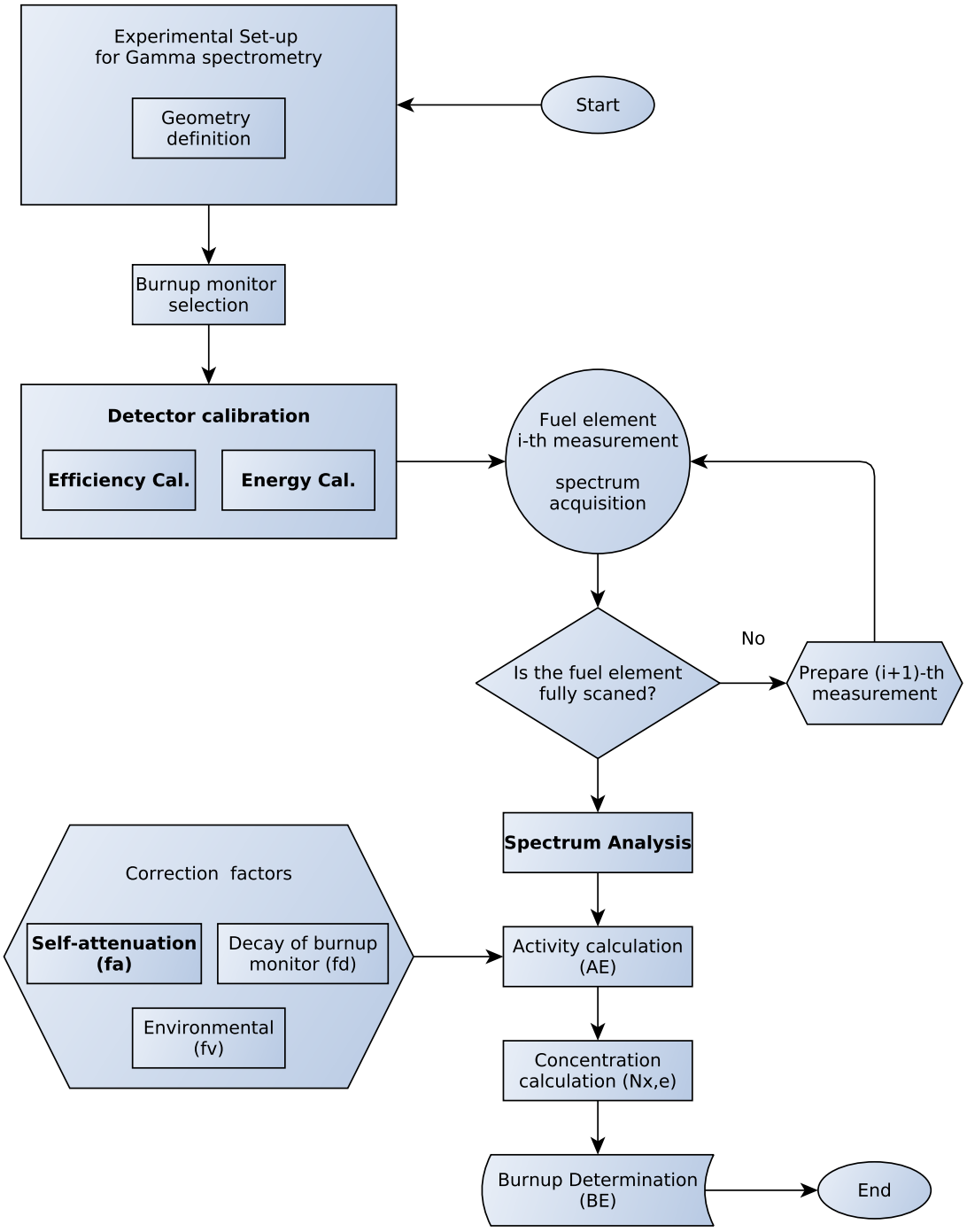

Figure 4.9: Experimental fuel burnup determination flowchart.

Chapter 5

Detector calibration

In this section, the calibration of a HPGe from the IJS is describe. The Canberra detector[1]: model GR2020 and serial number: b19809, has a crystal of 101.7 cm^3 with a relative efficiency of 20% for the FWHM resolutions of: 2.0 keV at 1.33 MeV and 1.10 keV at 0.122 MeV.

For the energy and efficiency calibration of the detector, a geometry similar to that of the experiment was proposed. See Figure 5.1.

The main characteristics of the point sources used for the detector calibration are described in Table 5.1.

The geometrical characteristics of the detector crystal are given in Figure 5.2.

5.1 Energy calibration

Gamma spectra measurements contains 8192 channels, for the detector previously mentioned, and show the number of counts in the photopeaks as a function of the channels they occupy, not providing any direct information about what is the gamma-ray energy that originated a certain photopeak in the obtained spectrum. Therefore, the energy calibration was performed as a function of the channel number, to be able to identify in each gamma spectrum the photopeaks corresponding to the gamma rays emitted in the decay of the burn monitors.

This is known as an energy calibration, and is performed by removing the detector from

[1]Technical information taken from the equipment *Certificate of conformity*, dated 05.05.2021.

the shielding and using the calibrated point sources presented in Table 5.1. Since the energy of the gamma-rays emitted by the calibration sources are well known and, knowing the position of each of the respective photopeaks, a linear function of the form $m \cdot x + b$ was adjusted to the energy as a function of the channel, see Table 5.3 and Figure 5.3.

It is worth noticing that a given calibration in energy is only valid for certain fixed conditions of adjustment of the electronic components of the experimental apparatus for the gamma-spectrometry, and it must be completely redone if these conditions are changed.

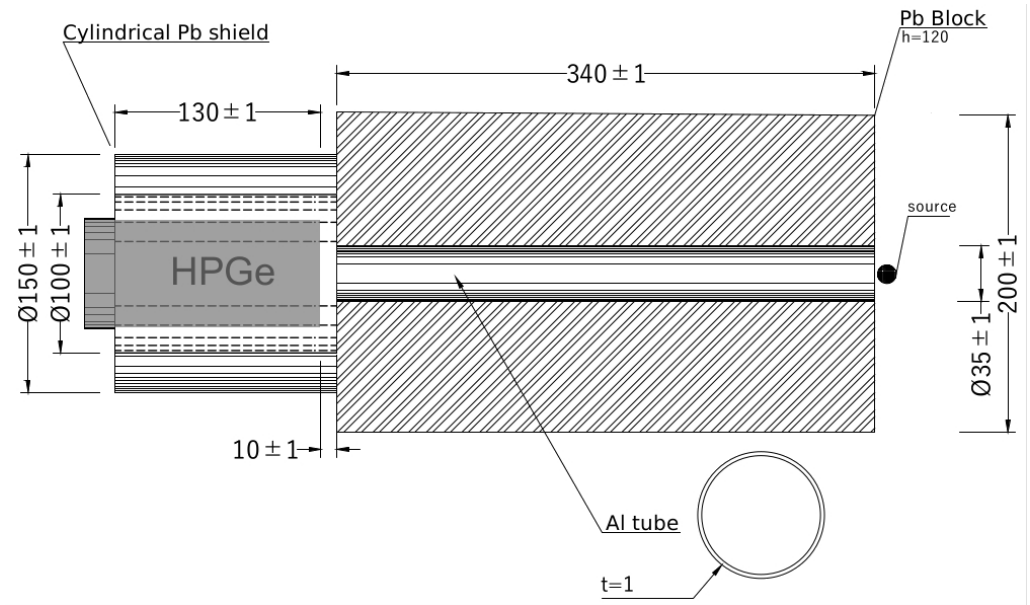

(a) Schematic of the experimental calibration setup.

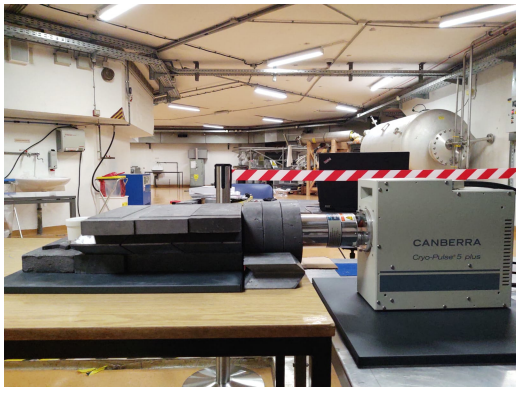

(b) Experimental setup lateral view.

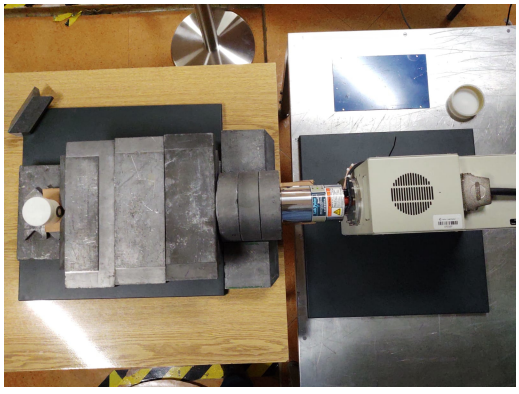

(c) Experimental setup aerial view.

Figure 5.1: Experimental acquisition setup for the detector calibration, at the IJS reactor facility. All the measurements are given in mm.

Table 5.1: Main characteristics of the point calibration sources. Where $T_{1/2}$ is the half-life, E_γ and I_γ are the respectively energy and emission intensity of the main emitted gamma rays and, A_0 the initial activity of the calibration source [25, 48, 49, 50, 51, 52, 53].

Calibration Source	$T_{1/2}$	E_γ [keV]	I_γ [%]	A_0 [kBq]	Reference date
^{133}Ba	10.55(1) y	80.998(1)	32.9(3)	236(4)	01.01.1990
		276.3989(12)	7.16(5)		
		302.8508(5)	18.34(13)		
		356.0129(7)	**62.05(10)**		
		383.8485(12)	8.94(6)		
^{137}Cs	30.08(9) y	**661.657(3)**	**85.10(20)**	39.7(7)	15.06.1988
^{60}Co	5.2711(4) y[a]	1173.228(3)	99.85(3)	476(12)	13.06.1995
		1332.492(4)	**99.983(1)**		
^{152}Eu	13.517(9) y	**121.7817(3)**	**28.53(16)**	216(4)	01.01.1990
		244.6974(8)	7.55(4)		
		344.2785(12)	26.59(20)		
		778.9045(24)	12.93(8)		
		964.057(5)	14.51(7)		
		1085.837(10)	10.11(5)		
		1112.076(3)	13.67(8)		
		1408.013(3)	20.87(9)		
^{226}Ra	1600(7) y	**186.211(13)**	**3.64(4)**	165(3)	01.01.1990
^{226}Ra/ ^{214}Pb[b]	27.06(7) min	241.9950(23)	7.251(16)		
		295.2228(18)	18.42(4)		
		351.9321(18)	**35.60(7)**		
^{226}Ra/ ^{214}Bi[b]	19.9(4) min	**609.320(5)**	**45.49(16)**		
		768.360(5)	4.894(11)		
		934.056(6)	3.107(10)		
		1120.294(6)	14.92(3)		
		1238.122(7)	5.834(15)		
		1377.669(8)	3.988(11)		
		1764.491(10)	15.30(3)		
^{241}Am	432.6(7) y	26.3446(2)	2.27(12)	37.9(8)	15.06.1988
		59.5409(1)	**35.9(4)**		

[a] Considering a year as 365.25 days.
[b] Short-live radionuclide from the ^{226}Ra decay chain.

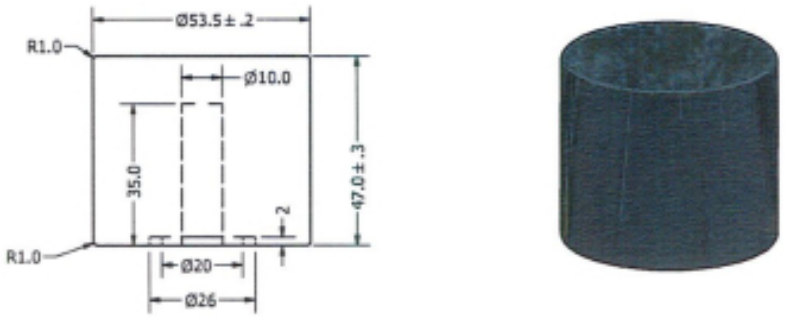

(a) HPGe crystal, geometrical parameters.

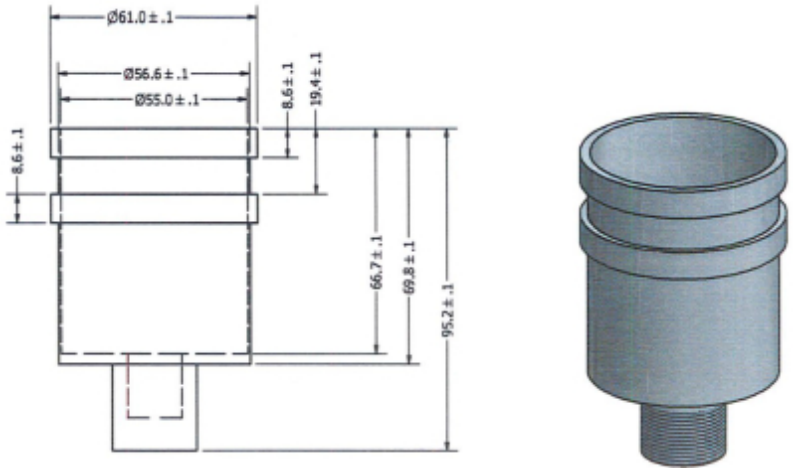

(b) HPGe holder, geometrical parameters. Material: Aluminum.

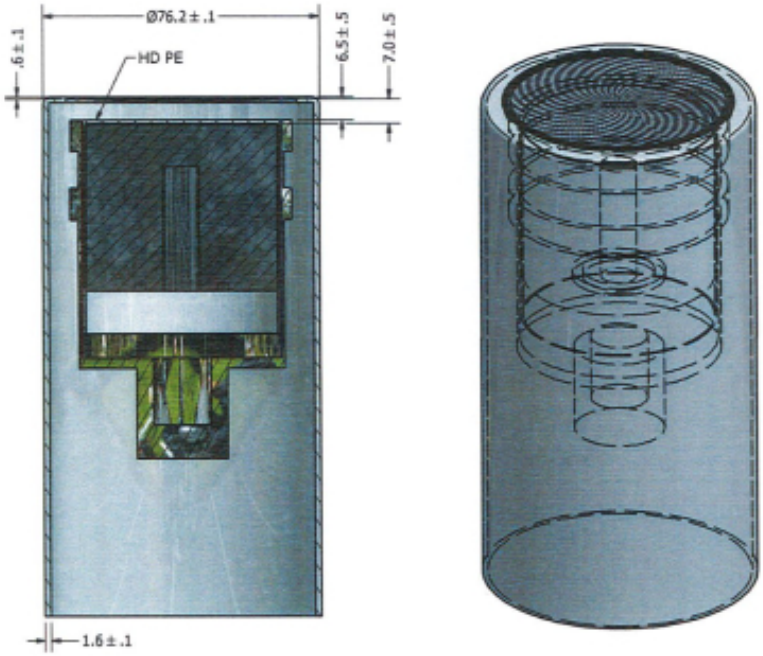

(c) HPGe assembly, geometrical parameters.

Figure 5.2: Technical drawing of the HPGe Canberra detector. All measurements are given in mm [54].

5.2 Efficiency calibration

To determine the experimental efficiency of a particular detector is done by establishing a fixed geometry, see Figure 4.4, and preserving the absorption and scattering characteristics of the experimental arrangement. The experimental intrinsic efficiency is calculated by [8, 30],

$$\epsilon_e = \frac{C_c/t_c}{G \cdot (I_c A_0 e^{-\lambda_c \cdot t_d^c})} \tag{5.1}$$

where ϵ_e is the experimental intrinsic efficiency, C_c are the total photo-peak counts of the measurements taken during the calibration, G is the geometrical correction factor and is related to the solid angle subtended due to the experimental calibration-geometry, I_c is the emission intensity of the characteristic photon from the radionuclide used for the calibration, A_0 is the initial activity of the certified calibration source, λ_c is the decay constant from the source, all of the previous from a certified calibration source, t_d^c is the decay time from the certification of the source to the acquisition of the spectra, and t_c is the counting of the live time for the spectrum acquisition. The term inside parenthesis in equation (5.1), is detonated as A_{theo} in Table 5.2.

The geometrical factor G due to a point source and a collimated circular cylindrical detector is given by [8],

$$G = \frac{\Omega}{4\pi} = \frac{1}{2}\left(1 - \frac{r_{sd}}{\sqrt{r_{sd}^2 + r_d^2}}\right) \tag{5.2}$$

where r_{sd} is the source-detector distance and, r_d is the collimator radius, see Figure 5.1a.

The calculated intrinsic efficiencies as function of the energy $\epsilon_{e,c}(E)$, are obtained from a general function of the form [30],

$$\epsilon_{e,c}(E) = a_0 + a_1\left[ln\left(\frac{E}{1400}\right)\right] + a_2\left[ln\left(\frac{E}{1400}\right)\right]^2 + a_3\left[ln\left(\frac{E}{1400}\right)\right]^3 \tag{5.3}$$

where E is the energy given in keV and, a_0, a_1, a_2 and a_3 are fitting parameters.

The Relative Intrinsic Error (ERI), for the calculated intrinsic efficiency is given by the

equation,

$$ERI = \frac{\epsilon_{e,c} - \epsilon_e}{\epsilon_e} \tag{5.4}$$

Table 5.2: Experimental intrinsic efficiency calibration data, for the intrinsic efficiencies ϵ_e, as function of gamma-energy from the calibration sources.

Source	E [KeV]	A_{theo}[a][Bq]	C_c/t_c [CPS]	ϵ_e
^{133}Ba	276.3989(12)	(2118 ± 35)	0.772(8)	0.25(3)
	302.8508(5)	(5426 ± 90)	1.83(8)	0.23(1)
	356.0129(7)	(18358 ± 278)	5.2(2)	0.195(7)
	383.8485(12)	(2645 ± 44)	0.71(7)	0.18(2)
^{137}Cs	661.657(3)	(15746 ± 244)	3.2(3)	0.138(12)
^{60}Co	1173.228(3)	(15250 ± 381)	1.83(9)	0.082(4)
	1332.492(4)	(15270 ± 382)	1.57(13)	0.070(6)
^{152}Eu	121.7817(3)	(12187 ± 195)	6.4(3)	0.361(14)
	244.6974(8)	(3225 ± 51)	1.31(11)	0.28(2)
	344.2785(12)	(11358 ± 191)	3.33(9)	0.200(8)
	778.9045(24)	(5523 ± 90)	0.87(6)	0.108(9)
	964.057(5)	(6198 ± 98)	0.80(4)	0.089(6)
	1085.837(10)	(4318 ± 68)	0.54(5)	0.085(9)
	1112.076(3)	(5839 ± 94)	0.67(6)	0.079(8)
	1408.013(3)	(8915 ± 139)	0.83(6)	0.064(5)
^{226}Ra	1764.491(10)	(24902 ± 392)	1.85(9)	0.051(3)
G= 0.00146(4)				
Fitting parameters				
model		Eq.(5.3)		
a_0		6.5219$\times 10^{-2}$		
a_1		-5.4522$\times 10^{-2}$		
a_2		4.4264$\times 10^{-2}$		
a_3		6.7280$\times 10^{-3}$		

[a] Theoretical activity corrected to the day of measurement (10.08.2021) and taking into account the gamma emission intensity for the given gamma-ray energy.

5.3 Results and discussion, calibration

The acquired spectrums from each of the nuclide used for the calibration process, are given in appendix B.2. The processed data output from the acquired spectrums for the efficiency calibration, is given in appendix B.3.1.

The spectrometry characterization results are presented. These are the measured detector intrinsic efficiency, see Table 5.2 and Figure 5.4. And the detector energy calibration, see Table 5.3 and Figure 5.3.

The efficiency calibration was done in the range $> 100\ keV$ since all the radionuclides of interest, see Table 4.1, are above this threshold. The intrinsic efficiency calibration data, see Figure 5.4, follows the shape expected from the literature [30, 43].

The model given by equation (5.3) and, the a_i parameters from Table 5.2, has an experimental range from 121.7 keV to 1764.5 keV, with a maximum and minimum ERI of 7.26% and -8.17% respectively.

Calculated intrinsic efficiencies $\epsilon_{e,c}$, for the selected burnup monitors gamma-energies are presented on Table 5.4, the errors of the calculated efficiencies are conservatively assumed by the maximum absolute value of the ERIs obtained from the model, i.e., 8.17%.

From the experimental point of view, it is recognized that the mayor cause of experimental uncertainty comes from the error of the C_c/t_c factor, the counting rate, from equation (5.1), with a range from 2.63% to 10.9%. The factor C_c that is the counts under the curve from the spectrometry analysis, it is directly influenced by the activity of the calibration source at the moment of the data acquisition rather than by the acquisition time. The important quantity to take into account is the counting rate.

Another factor having great influence not on the final uncertainty of the efficiency, but on the quality of the measurements, is the geometrical factor G. The error contribution for the geometrical factor G is lower than 3% and with a lower noticeable influence to the final error of ϵ_e, than the one coming from the counting rate. The greater the geometrical factor, the higher the probability of detection of an event in the detector, therefore, the proper definition of this value has a great influence in said counting rate during the acquisition of the spectrum.

The activity of the calibration sources and, the definition of the geometrical factor becomes important for the quality of the calibration. The activity of these sources should be high enough and, the geometrical factor should have a value such that, allows to have a good counting rate but lower enough that the value of the detectors dead-time still allow to neglect undesired events such as the sum-coincidence[2] effects in the spectrum.

[2]Also known as pulse pileup. Is when two independent events arrive faster than the resolution time of the detector and are recognized as one event, i.e., overlapping of the signals [8].

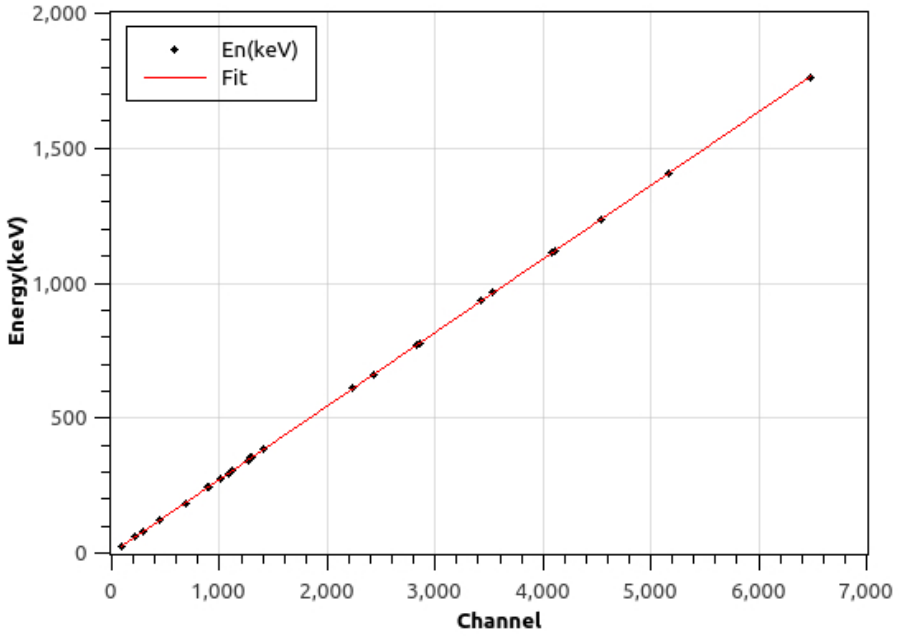

Figure 5.3: Energy calibration plot. Data from Table 5.3. See Listing C.5, for the fitting results.

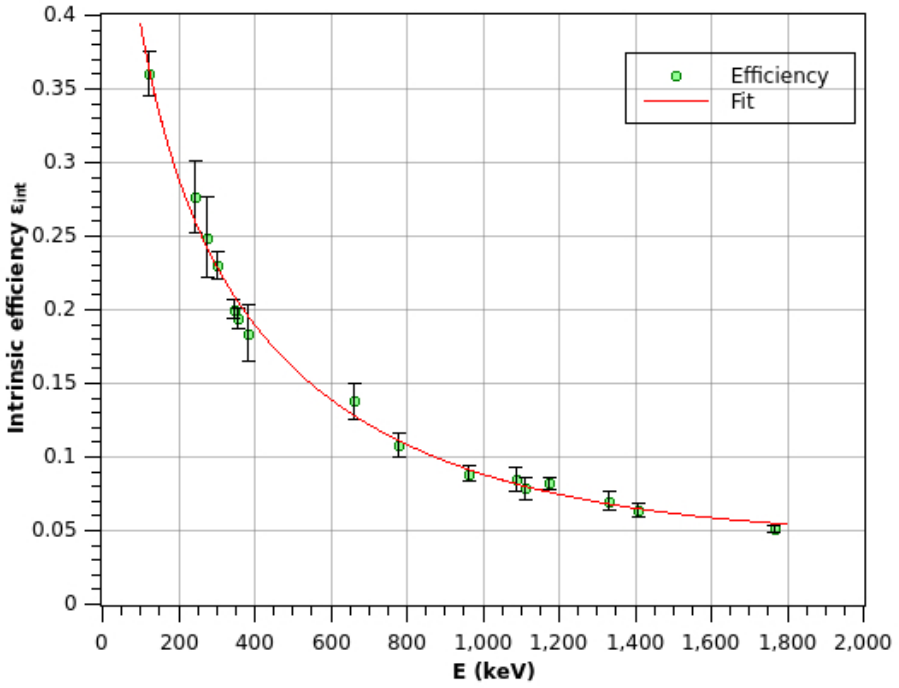

Figure 5.4: Measured intrinsic efficiencies as a function of energy from the gamma-rays from the calibration sources for the range from 121.7 keV to 1764.5 keV, with a maximum and minimum relative intrinsic error with respect to the data from Table 5.2, of 7.26% and -8.17% respectively. See Listing C.6, for the fitting results.

Table 5.3: Channel-energy data for the energy calibration of the detector.

Source	E [KeV]	Channel
^{133}Ba	80.998(1)	296.78(12)
	276.3989(12)	1013.97(12)
	302.8508(5)	1111.07(8)
	356.0129(7)	1306.14(8)
	383.8485(12)	1408.44(14)
^{137}Cs	661.657(3)	2428.42(7)
^{152}Eu	121.7817(3)	446.37(2)
	244.6974(8)	897.54(8)
	344.2785(12)	1263.12(7)
	778.9045(24)	2858.7(2)
	964.057(5)	3538.1(3)
	1112.076(3)	4081.8(3)
	1408.013(3)	5167.9(4)
^{226}Ra	186.211(13)	682.86(8)
^{226}Ra/ ^{214}Pb	241.9950(23)	887.73(4)
	295.2228(18)	1083.08(5)
	351.9321(18)	1291.231(15)
^{226}Ra/ ^{214}Bi	609.320(5)	2236.27(5)
	768.360(5)	2819.9(4)
	934.056(6)	3428.6(4)
	1120.294(6)	4112.0(4)
	1238.122(7)	4544.3(4)
	1764.491(10)	6476.8(3)
^{241}Am	26.3446(2)	96.53(5)
	59.5409(1)	218.13(2)
Fitting parameters		
model	$y(x) = m \cdot x + b$	
m	0.27241	
b	0.16129	

Table 5.4: Calculated intrinsic efficiencies ϵ_e, using equation (5.3) and fitting parameters from Table 5.2. The ϵ_e values obtained, are for the gamma energies from the selected burnup monitors from Table 4.1.

BU Monitor	E [keV]	$(\epsilon_e \pm 8.17\%)$
^{137}Cs/^{137m}Ba	661.6	0.1281
^{95}Zr	724.2	0.1184
	756.7	0.1139
^{140}Ba/ ^{140}La	1596.5	0.0588
^{144}Ce/ ^{144}Pr	2185.7	0.05030[a]

[a] Extrapolated value.

Chapter 6

Summary

Basic concepts related to nuclear engineering, gamma-spectroscopy and, fuel burnup were introduced, as well as some of the main reasons that motivates the burnup calculations, such as fuel economics, safety analysis and, safeguards. An introduction to the Slovenian Mark TRIGA II reactor was given, together with a description of the nuclear fuel used by a TRIGA reactor and, the main characteristics from an average fuel element from the Slovenian TRIGA reactor. The fission products obtained from the TRIGA fuel, the main gamma-emitters from said fission-products together with their important characteristics for the realization of the gamma spectroscopy technique, were presented on Table 2.2.

The model for the theoretical burnup estimation from a selected fission product was developed, see Section 2.3. This model encompass the estimation of: the theoretical concentration, see equation (2.15); the activity, see equation (2.18), the relevant correction factors for its estimation, see Section 2.3.2 and; the burnup given in units of mass, see equation (2.22), for a TRIGA nuclear fuel element.

A Brief explanation for the different types of assays and related techniques used for the fuel burnup determination were presented. This includes destructive, see Section 3.1 and non-destructive methods, see Section 3.2. Later, from the non-destructive-assays the gamma spectroscopy technique was introduced alongside with the advantages and disadvantages of said technique, see Section 4.1. Also, the main characteristics that a fission product must have to be considered experimentally as a good burnup monitor were presented, see Section 4.2 and, the more suitable radionuclides matching said characteristics were given, see Table 4.1.

An overview of the experimental steps necessary for the fuel burnup determination by the

gamma-spectroscopy technique was presented. To do so, it was assumed that the experiment will be carried out in the spent-fuel pool and the characteristics of said geometry were described generically, see Figure 4.4. Some key aspects related to the experimental correction factors required the development of analytical models, such as: the self-attenuation coefficient of the nuclear fuel, see equation (4.8), including the TRIGA fuel materials attenuation coefficients for the U-ZrH fuel mixture, see equation (4.9) and the SS-304 cladding alloy, see equation (4.10) and; the environmental attenuation coefficient, see equation (4.13). A list of values for the self-attenuation coefficient, using the energies of the proposed burnup monitors, was estimated for an average fuel element from the Slovenian TRIGA reactor, see Table 4.2.

Assuming an already processed spectrum, the experimental activity, see equation (4.14); concentration, see equation (4.17) and; fuel burnup estimation, see equation (4.18); were presented. Some possibles sources of experimental uncertainty and ways to avoid them were briefly listed and, a workflow for the experiment was suggested.

The obtained energy and efficiency calibration factors from a High-Purity Germanium detector calibrated at the Institute "Jozef Stefan" were presented, see Section 5.3.

To accomplish the calibration, a computational tool for the spectral analysis was developed in matlab, see appendix B.3, alongside with the procedure for the conversion of the proprietary files from the detector to plain text files, see appendix B.1.

The spectral analysis includes finding the photo-peaks centroids, the area under the curve, the Full-Width-at-Half-Maximum, the background height, the coefficient R^2 from the goodness-of-fit test and, the date of the measurement; Also the plot for each found peak is generated as an image file. See appendix B.3.1, for the spectral analysis output files content.

Chapter 7

Discussion and conclusion

Applying the reasons given in Section 2.1, together with the different techniques presented in Chapter 3, would open up a range of possibilities for future researches at the IJS.

Of these possible researches, some have already been previously implemented at the IJS, nevertheless, they can serve as a starting point for comparison of future projects. At the moment, there is a particular interest in the development of the gamma spectrometry technique at the IJS, hence the origin of this work. Due to this, not only the knowledge of the gamma-spectrometry technique was deepened. Also, was deepened the requirements for the ancillary equipment, such as the ones presented in Figure 4.4 as well as, the optimum fission products to perform the experiment in a reliable way.

The above, was possible by combining the diverse knowledge and experiences mostly from the Latin-American, North-American and European regions. The presented cumulative expertise acquires over the years, in a quite diverse number of languages, allows us now, to have a better idea of what to expect during the execution of the fuel burnup determination employing the gamma-spectroscopy technique, to be carried out at the IJS. It is worth mention that for this work only the scientific/technical area was considered, however, it should not be forgotten that this goes hand-in-hand with regulatory requirements that must be fully taking care of. This is the main reason why a generalized case is presented in Section 4.5, for the experimental setup, so it can be adapted to the technical and, regulatory requirements; relevant to the IJS and, the Republic of Slovenia, respectively.

Regarding the gamma-spectrometry analysis of nuclear fuel elements, the lessons learned during the calibration of the detector can be extrapolated, this lead to the important role that the counting rate play in the development of the experiment and, how it should be

carefully calibrated for the acquisition of the data utilizing the solid angle, the source-detector distance or adding extra photon-absorption material, i.e., more water; all of this to reduce or increase, the counting rate at the detector to improve the counting statistics.

The development of alternatives to commercial software, was also carried out for the analysis of the acquired spectrums.

For any future work the following elements, according to the workflow suggested in Figure 4.9, were fully developed and can be used right away:

- Detector calibration, energy and efficiency.
- Spectrum analysis tool, using the Matlab code.
- The mass attenuation coefficients equations for U-ZrH and SS304.
- The calculated values for the fuel self-attenuation coefficient.

7.1 Future work

For the future work related to this topic at the IJS, it is planned to build the necessary equipment, such as the ones presented in Figure 5.1, and compare the results obtained with the ongoing Monte Carlo simulation research based on the detailed records keep by the reactor operators through the many decades of the reactor operation.

References

[1] A. Peršič, T. Žagar, M. Ravnik, S. Slavič, B. Žefran, D. Ćalić, A. Trkov, G. Žerovnik, A. Jazbec and L. Snoj, *TRIGLAV: A program package for TRIGA reactor calculations*, Nuclear Engineering and Design **318**, 10.1016/j.nucengdes.2017.04.010 (2017).

[2] W. Huda and R. Slone, *Review of radiologic physics*, 2nd ed. (Lippincott williams & Wilkins, 2002).

[3] The Editors of Encyclopaedia, *"Cross section"*. *Encyclopedia Britannica*, [Acceced 4. 3. 2021], available at `https://www.britannica.com/science/cross-section-physics`.

[4] Unknown, *"Neutron Flux"*. *U.S.NRC Library, Basic References* (), [Acceced 15. 3. 2021], available at `https://www.nrc.gov/reading-rm/basic-ref/glossary/neutron-flux.html`.

[5] G. Bell and S. Glasstone, *Nuclear Reactor Theory* (Van Nostrand Reinhold, 1970).

[6] S. Glen, *"Gamma ray"*. *Encyclopedia Britannica*, [Acceced 4. 3. 2021], available at `https://www.britannica.com/science/gamma-ray`.

[7] P. Bevington and K. Robinson, *Data reduction and error analysis for physical sciences*, 3rd ed. (McGraw-Hill, 2002).

[8] G. F. Knoll, *Radiation Detection and Measurement*, 4th ed. (Wiley, 2010).

[9] N. Tsoulfanidis, *Measurement and Detection of Radiation*, 2nd ed. (Taylor & Francis, 1995).

[10] J. E. Turner, *Atoms, Radiation, and Radiation Protection*, 3rd ed. (Wiley-VCH, 2007).

[11] D.Vénos, A. V. A.-V. Geert, N. Severijns, D. Srnka and D. Zákoucký, *The behaviour of HPGe detectors operating at temperatures below 77 K*, Nuclear Instruments and Methods in Physics Research Section A: Accelerators, Spectrometers, Detectors and Associated Equipment **454**, 10.1016/s0168-9002(00)00494-0 (2000).

[12] P. A. Valenzuela, *Estudio experimental del quemado de combustible nuclear por el método de espectrometría gamma*, Master's thesis, Facultad de Ciencias, Universidad Autónoma del Estado de México (2009).

[13] J. R. Taylor, *An Introduction to Error Analysis: The Study of Uncertainties in Physical Measurements*, 2nd ed. (University Science Books, 1997).

[14] J. R. Lamarsh, *Introduction to Nuclear Reactor Theory*, 1st ed. (American Nuclear Society, 2002).

[15] V. V. Rondinella and T. Wiss, *The high burn-up structure in nuclear fuel*, Materials Today **13**, 10.1016/s1369-7021(10)70221-2 (2010).

[16] Unknown, *"Backgrounder: On High Burnup Spent Nuclear Fuel". U.S.NRC Library* (), [Acceced 11. 4. 2021], available at `https://www.nrc.gov/reading-rm/doc-collections/fact-sheets/bg-high-burnup-spent-fuel.html`.

[17] D. Olander, *Fundamental Aspects of Nuclear Reactor Fuel Elements*, 1st ed. (Technical Information Center, 1976).

[18] J. J. Duderstadt and L. J. Hamilton, *Nuclear Reactor Analysis*, 1st ed. (Wiley, 1976).

[19] J. R. Lamarsh and A. J. Baratta, *Introduction to Nuclear Engineering*, 3rd ed. (Prentice Hall, 2001).

[20] J. C. Wagner and M. D. DeHart, *Review of Axial Burnup Distribution Considerations for Burnup Credit Calculations* 10.2172/763169 (2000).

[21] M. Tardy, S. Kitsos, G. Grassi, A. Santamarina, L. S. Felice and C. Riffard, *First burnup credit application including actinides and fission products for transport and storage cask by using French experiments*, Journal of Nuclear Science and Technology **52**, 10.1080/00223131.2015.1037808 (2015).

[22] P. Juutilainen and S. Häkkinen, *Impact of fuel type and discharge burnup on source term*, in *Proceedings* (2019) 28th International Conference Nuclear Energy for New Europe, NENE 2019.

[23] K. L. Nash and G. J. Lumetta, *Advanced Separation Techniques for Nuclear Fuel Reprocessing and Radioactive Waste Treatment*, 1st ed., Series in Energy (Woodhead Publishing, 2011).

[24] Ž. Štancar, L. Snoj and L. Barbot, *Reaction rate distribution experiments at the Slovenian JSI TRIGA Mark II research reactor*, International Handbook of Evaluated Reactor Physics Benchmark Experiments. TRIGA-FUND-RESR-002 Paris (2017).

[25] J. Laurec, A. Adam, T. de Bruyne, E. Bauge, T. Granier, J. Aupiais, O. Bersillon, G. Le Petit, N. Authier and P. Casoli, *Fission Product Yields of 233U, 235U, 238U and 239Pu in Fields of Thermal Neutrons, Fission Neutrons and 14.7-MeV Neutrons*, Nuclear Data Sheets **111**, 10.1016/j.nds.2010.11.004 (2010).

[26] B. R. T. Frost, *Nuclear Fuel Elements. Design, Fabrication and Performance*, 1st ed. (Pergamon Press, 1982).

[27] C. A. Zeituni, *Espectrometria gama en elementos cobustíveis tipo placa irradiados*, Master's thesis, Instituto de Pesquisas Energéticas e Nucleares (IPEN), Autarquia associada à Universidade de São Paulo (1998).

[28] D. Olander, E. Greenspan, H. D. Garkisch and P. B., *Uranium–zirconium hydride fuel properties*, Nuclear Engineering and Design **239**, 10.1016/j.nucengdes.2009.04.001 (2009).

[29] M. Simnad, *The U-ZrHx alloy: Its properties and use in TRIGA fuel*, Nuclear Engineering and Design **64**, 10.1016/0029-5493(81)90135-7 (1981).

[30] L. Terremoto, C. Zeituni, J. Perrotta and J. da Silva, *Gamma-ray spectroscopy on irradiated MTR fuel elements*, Nuclear Instruments and Methods in Physics Research Section A: Accelerators, Spectrometers, Detectors and Associated Equipment **450**, 10.1016/s0168-9002(00)00250-3 (2000).

[31] *Determination of Research Reactor Fuel Burnup*, TECDOC Series No. 633 (International Atomic Energy Agency (IAEA), Vienna, 1991).

[32] F. L. Lisman, W. J. Maeck and J. E. Rein, *Determination of Nuclear Fuel Burnup from Fission Product Analysis*, Nuclear Science and Engineering **42**, 10.13182/nse70-a19501 (1970).

[33] J.-S. Kim, S.-H. Han, M.-Y. Suh, K.-S. Joe and T.-Y. Eom, *Burnup measurement of irradiated uranium dioxide fuel by chemical methods*, Nuclear Engineering and Technology **21**, 277 (1989).

[34] J. M. Harp, P. A. Demkowicz, P. L. Winston and J. W. Sterbentz, *An analysis of nuclear fuel burnup in the AGR-1 TRISO fuel experiment using gamma spectrometry, mass spectrometry, and computational simulation techniques*, Nuclear Engineering and Design **278**, 10.1016/j.nucengdes.2014.07.041.

[35] I. C. Gauld, M. L. Williams, F. Michel-Sendis and J. S. Martinez, *Integral nuclear data validation using experimental spent nuclear fuel compositions*, Nuclear Engineering and Technology **49**, 1226 (2017).

[36] M. Gysemans, *Radiochemical analysis of nuclear fuel burn-up and spent fuel key nuclides (INIS-BE–0010)*, SCK-CEN Progress Report 2005 , 77 (2006).

[37] T. Cran, *Nondestructive assay methods for irradiated nuclear fuels*, LA-6923 (1978).

[38] M. Pusa, *Numerical methods for nuclear fuel burnup calculations*, Doctoral thesis, Aalto University, School of Science (2013).

[39] M. Ravnik, M. Strebl, H. Böck, A. Trkov and I. Mele, *Determination of the burn-up of TRIGA fuel elements by calculation and reactivity experiments*, Kerntechnik **57**, 291 (1992).

[40] A. Zuñiga, T. Baldo and M. Ravnik, *APPLICATION OF REACTIVITY METHOD TO MTR FUEL BURN-UP MEASUREMENT*, Informe Científico Tecnológico 1998-2001. Lima: IPEN (2002).

[41] W. Tien-Ko, H. De-Chiun and T. Chia-Lian, *Feasibility studies on iterative methods of fuel burnup estimation using gamma-ray spectrometry*, International Journal of Radiation Applications and Instrumentation. Part A. Applied Radiation and Isotopes **41**, 10.1016/0883-2889(90)90128-4 (1990).

[42] F. H. Attix, *Introduction to Radiological Physics Radiation Dosimetry*, 1st ed. (Wiley-VCH, 1986).

[43] S. Bagheri and H. Khalafi, *The irradiated fuel-burnup experiment of Tehran Research Reactor using nondestructive gamma-ray spectroscopy*, Applied Radiation and Isotopes **167**, 109444 (2021).

[44] A. Kestelman and S. Ribeiro-Guevara, *Determinación del Quemado en Combustibles tipo MTR mediante Espectrometría Gamma con Cristal de NaI(TI)*, Informe Comisión Nacional de Energía Atómica (CNEA), 497. Argentina (1988).

[45] M. Vela, M. Nieto and J. Guarnizo, *Aplicación del método de espectrometría gamma para determinar el quemado de un elemento combustible del reactor RP-10*, Informe Científico Tecnológico 1998-2001. Lima: IPEN (2002).

[46] M. vela, A. Padilla, J. Palomino and L. Terremoto, *Nondestructive burnup measurements by gamma-ray spectroscopy on spent fuel elements of the RP-10 research reactor*, Progress in Nuclear Energy **53**, 344 (2011).

[47] M. Berger, J. Hubbell, S. Seltzer, J. Chang, J. Coursey, R. Sukumar, D. Zucker and K. Olsen, *XCOM: Photon Cross Section Database. version 1.5 (2010). National Institute of Standards and Technology*, [Acceced 29. 4. 2021], available at `http://physics.nist.gov/xcom`.

[48] M. Basunia, *NuDat 2.6*, Nuclear data sheets **107**, 3323 (2006).

[49] E. Browne and J. Tuli, *Nuclear data sheets for A= 137*, Nuclear Data Sheets **108**, 2173 (2007).

[50] Y. Khazov, A. Rodionov and F. Kondev, *Nuclear data sheets for A= 133*, Nuclear Data Sheets **112**, 855 (2011).

[51] M. Martin, *Nuclear data sheets for A= 152*, Nuclear Data Sheets **114**, 1497 (2013).

[52] S. Singh, A. Jain and J. K. Tuli, *Nuclear data sheets for A= 222*, Nuclear Data Sheets **112**, 2851 (2011).

[53] S.-C. Wu, *Nuclear data sheets for A= 214*, Nuclear Data Sheets **110**, 681 (2009).

[54] Canberra Semiconductors NV., *MCNP-DATA [Technical Drawing]*, dwg No.OLE0015119, 2015.

[55] F. Aguilar, *Mexican TRIGA Mark-III Reactor*, in *History, Development and Future of TRIGA Research Reactors* (2016).

[56] A. Morales and F. Razo, *Reactor TRIGA MARK III del Centro Nuclear de México: Descripción, Construcción, Montaje y Operación*, Revista Mexicana de Física **19**, s27 (1970).

[57] W. Johnson and USDOE, *Cambio [Computer software]* (2015).

Appendix A

Fuel element theoretical analysis

A working example on how to properly do the theoretical burnup calculations is presented by means of a TRIGA III reactor FE.

The Mexican TRIGA Mark III reactor is located inside the Nuclear Center "Dr. Nabor Carrillo Flores". It is one of the main facilities of the *Instituto Nacional de Investigaciones Nucleares*[1] (**ININ**). The facility is surrounded by a forest and is located near the highway that joins Mexico City and Toluca City. The ININ reactor, is a pool-type research reactor with a mobile core that is cooled by the natural convection of the pool water. The maximum power in steady state is 1 MW in any position of the pool. Its first criticality was achieved on November 8, 1968 at 20:38 hours [55, 56].

The use of the main theoretical equations from Section 2.3, would be demonstrated by means of the analysis of a FE from the ININ reactor, specifically for the LEU fuel element *EC5091* with an initial $^{235}\mathrm{U}$ mass of m_u^0= 39.0 grams. The FE was subject to 4 ring positions changes during 11 core configurations, with an irradiation time of 269.24 days, and a cool-down period of 7846 days afterwards. These calculations would be directly compared with the experimental results from reference [12].

Isotope $^{137}\mathrm{Cs}$ was selected as the burnup monitor, due to the long cool-down time of the FE even though the irradiation time is less than 2 years. Therefore equation (2.15) become,

$$N_{cs}(t_i) = \frac{\sigma_u^f \phi Y_{cs} N_u}{\lambda_{cs} + \sigma_{cs}^c \phi} \left[1 - e^{-(\lambda_{cs} + \sigma_{cs}^c \phi) t_i}\right] \tag{A.1}$$

[1] National Institute for Nuclear Research

for the previous equation, the data from Table A.1 was used to calculate the N_{cs} concentration value, see Table A.4. For the positions inside the core of the ININ reactor the concentric rings are distributed and labeled as in Figure A.1.

Table A.1: Values used to estimate the ^{137}Cs concentration and the theoretical burnup [12].

Symbol	Value		comment
t_i	2.32623×10^7	(s)	269.24 days, irradiation time.
V_{fe}	294.78	(cm^3)	
ϕ	6.1509×10^{12}	(n/cm^2-s)	Average neutron flux at the dry cell.
N_u	2.53153×10^{20}	(atoms/cm^3)	From the initial ^{235}U mass and V_{fe}.
σ_u^f	580×10^{-24}	(cm^2)	
Y_{cs}	0.0626	$-$	
σ_{cs}^c	0.11×10^{-24}	(cm^2)	^{137}Cs capture cross-section.
λ_{cs}	7.3020×10^{-10}	(1/s)	From ^{137}Cs Half-life, 30.08 years.
M_u	235.04	(g/mol)	
N_A	6.022×10^{23}	(atoms/mol)	Avogadro number.
α	0.17	$-$	

The ith irradiation position, as explained in Section 2.3.2.2, is associated to the ring position were the FE was located during the m core configuration. See Table A.2.

Table A.2: Power factors $(P_F)_i$, per ring position (i) according to different m configurations for the ININ reactor [12].

core	$(P_F)_i$ per Ring				
Config. ID	B	C	D	E	F
1 to 9	1.52	1.34	1.16	0.89	0.73
10 to 13	1.50	1.24	1.14	0.97	0.77

Now, it is possible to estimate the *decay of burnup monitor* and the *average power* correction factor. Therefore equation (2.16) become

$$f_d = \frac{\lambda_{cs} \sum_{k=1}^{n} P_k \cdot t_k}{\sum_{k=1}^{n} P_k \cdot e^{-\lambda_{cs}\tau_k}[1 - e^{-(\lambda_{cs}+\sigma_{cs}^c\phi)t_k}]} \tag{A.2}$$

for the previous equation and for equation (2.17), the necessary values were taken from Table A.1 and Table A.3. For the final values of the correction factors, see Table A.4.

Table A.3: Values from the fuel element *EC5091* log-book, used to estimate the decay of burnup monitor and average power correction factors from the ININ reactor [12].

core config. ID	Power (MWd)	P_k	t_k (s)	$(P_F)_i$	τ_k (s)
1	17.41	0.0647	57801600	1.34	598449600
2	40.39	0.1500	89942400	1.34	524577600
3	10.7	0.0397	9072000	1.34	475070400
4	5.62	0.0209	5616000	1.34	467726400
7	5.05	0.0188	5011200	0.73	419644800
8	61.82	0.2296	90288000	0.73	371995200
9	6.17	0.0229	9072000	0.73	322315200
10	43.19	0.1604	76982400	1.24	279288000
11	41.55	0.1543	75859200	1.24	202867200
12	8.09	0.0300	13996800	1.24	157939200
13	29.25	0.1086	150940800	0.97	75470400
	$\sum$=269.24	$\sum$=1			

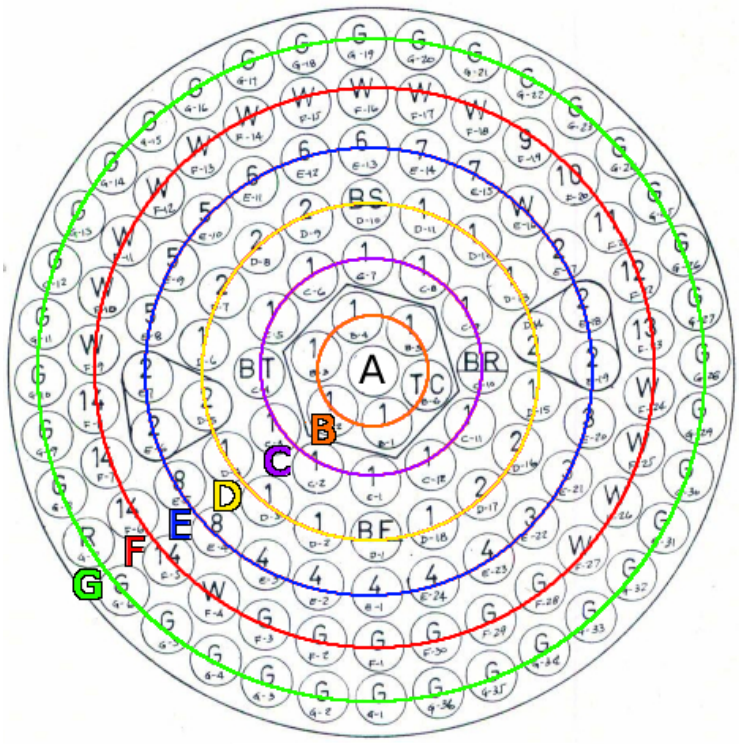

Figure A.1: Grid schematic from the ININ Mexican TRIGA reactor core with its ring labels [56].

The theoretical burnup equation (2.22) becomes,

$$B_T = \frac{(N_{cs}V_{fe})}{Y_{cs}} \frac{M_u}{N_A}(1+\alpha) \cdot f_d \cdot \overline{F_p} \tag{A.3}$$

for which the following data was used, see Table A.1. The results of the calculations and the comparison with the experimental burnup, taken from [12], can be found in Table A.4.

Table A.4: Values for the theoretical $^{137}\mathrm{Cs}$ concentration, correction factors, and burnup. As well as the comparison with the experimental value obtained.

N_{cs}	1.30404×10^{18}	(atoms/cm^3)
f_d	1.2881	
$\overline{F_d}$	1.0998	
B_T	5.31 g	
B_e	5.15(4) g	Data from ref. [12]

Appendix B

Spectrum analysis

The spectrums were taken with the detector described in Chapter 5. CAMBERRA detectors creates '.CNF' files to store the spectral measurement data recorded with the Genie 2000 radiation spectrometry software. Therefore, in order to analyze the data, these files need to be converted to a more suitable format.

B.1 File conversion: from CNF to TXT

The software used was *cambio*; version: cl_linux_x86_d3_20191022. This software converts spectrum files from nearly all common handheld and lab-based spectroscopic gamma radiation detectors, radiation portal monitors, or search systems to a format of your choice (N42, PCF, CSV, TXT, CHN, SPC, HTML, and more) [57].

B.2 Measured gamma-spectrums

In this section the plots of the measured spectrums used for the calibrations, after file conversion, are presented. The spectrums were measured under the geometry given in Chapter 5.

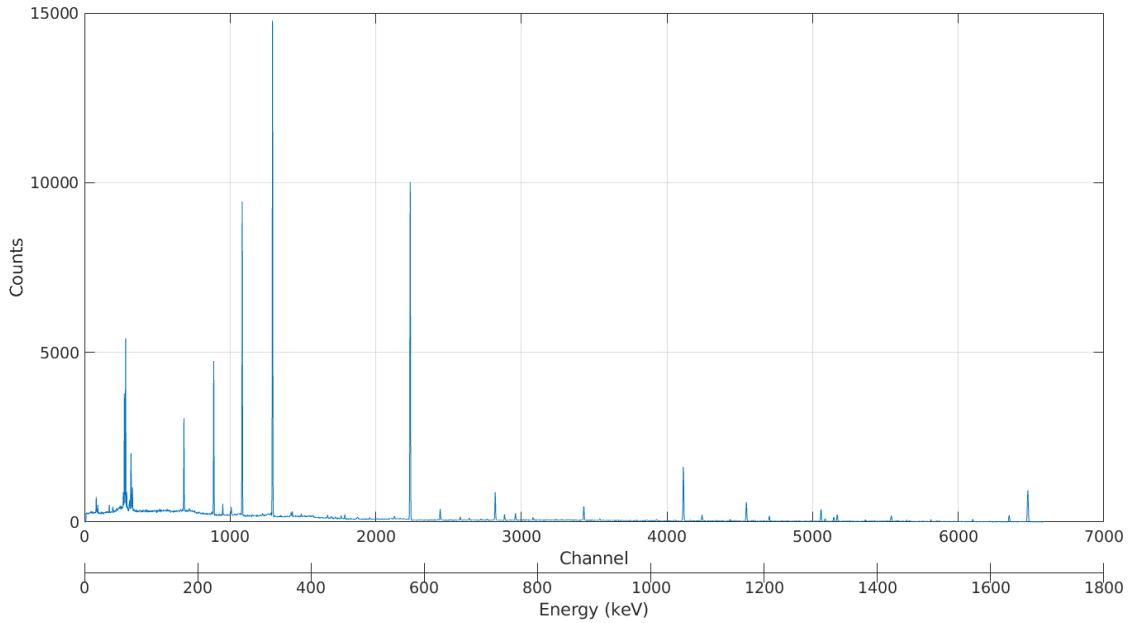

Figure B.1: Measured $^{226}\mathrm{Ra}$ spectrum.

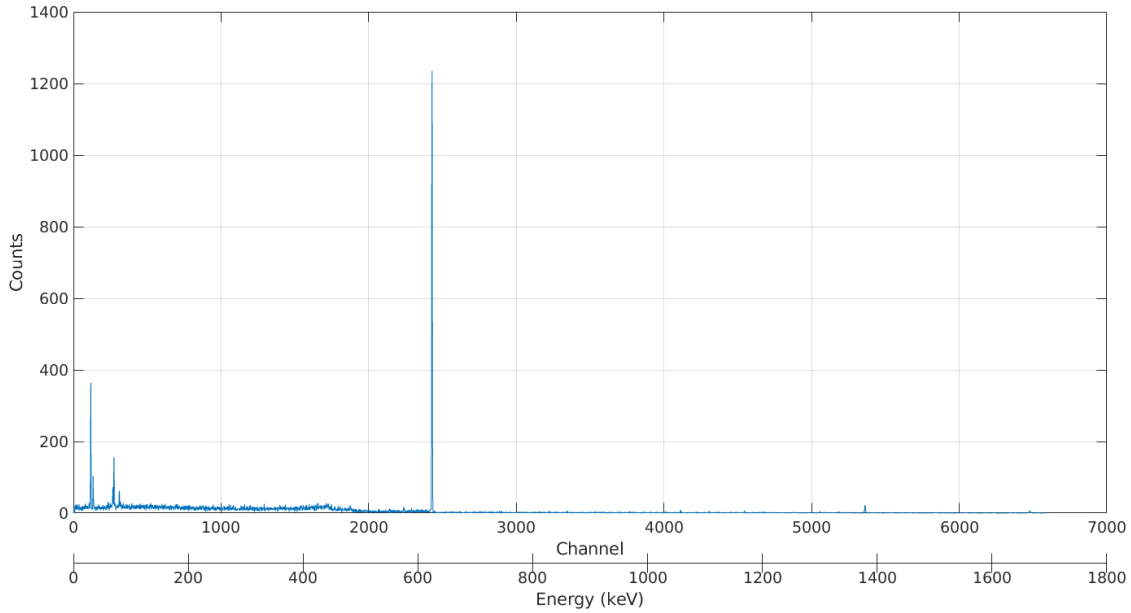

Figure B.2: Measured $^{137}\mathrm{Cs}$ spectrum.

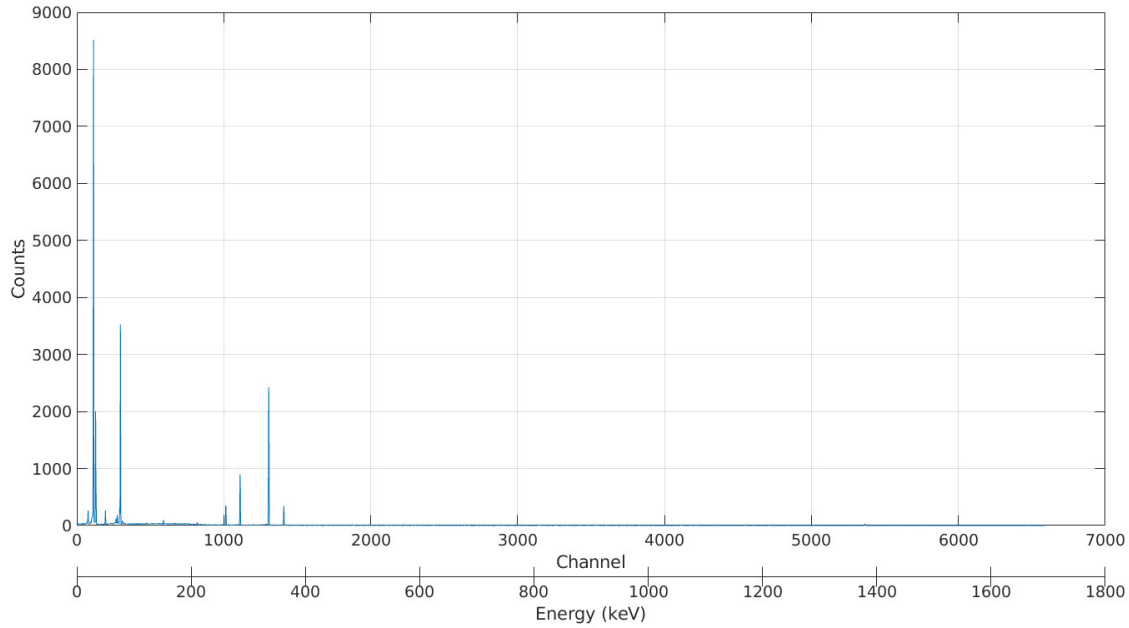

Figure B.3: Measured ^{133}Ba spectrum.

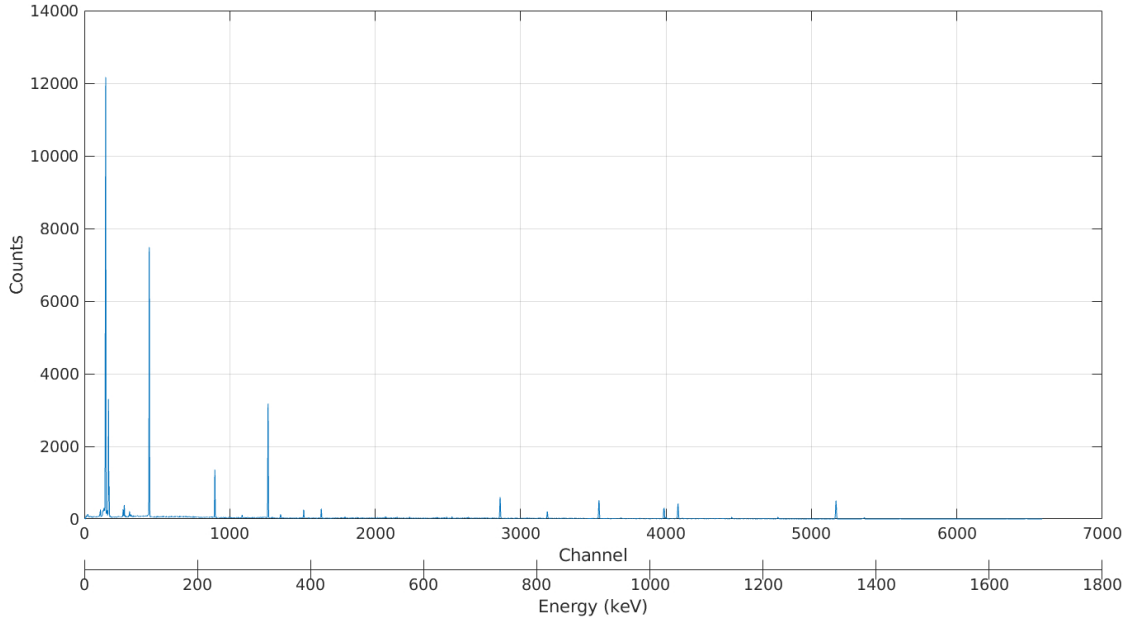

Figure B.4: Measured ^{152}Eu spectrum.

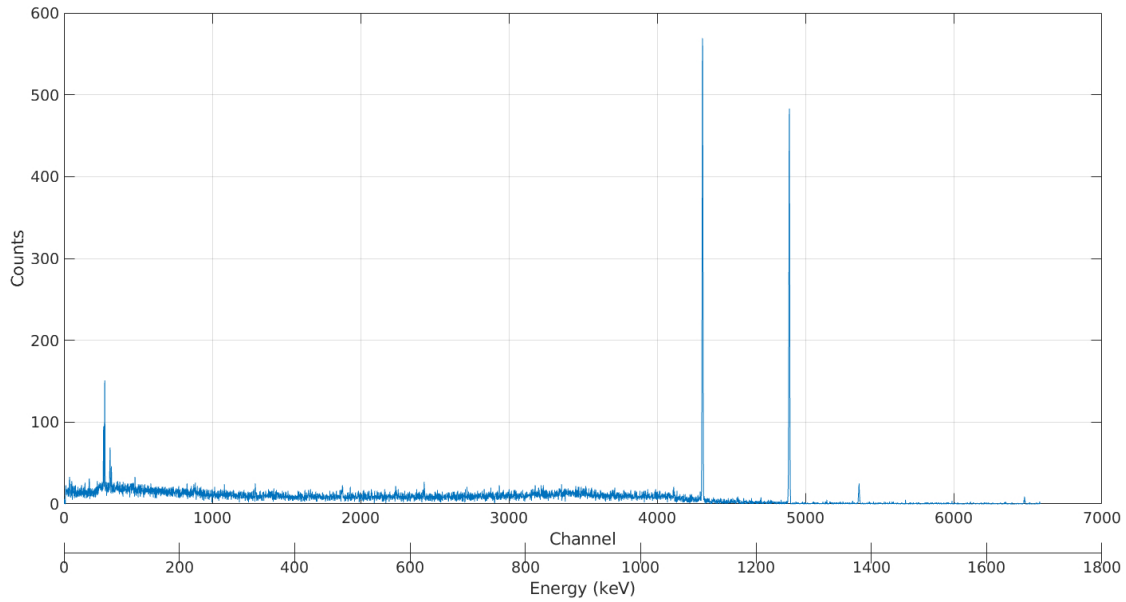

Figure B.5: Measured ^{60}Co spectrum.

B.3 Matlab code

The MATLAB version used for the analysis has the following characteristics:

- Version: 9.7.0.1319299 (R2019b) Update 5
- Operating System: Linux 4.15.0-147-generic #151-Ubuntu x86_64
- Java Version: Java 1.8.0_202-b08 with Oracle Corporation Java HotSpot(TM) 64-Bit Server VM mixed mode
- Necessary MATLAB APPS to run the scripts:
  - Simulink. Version 10.0
  - Curve Fitting Toolbox. Version 3.5.10
  - Signal Processing Toolbox. Version 8.3
  - Statistics and Machine Learning Toolbox. Version 11.6
  - Symbolic Math Toolbox. Version 8.4

Brief description of the MATLAB code used for the spectrum analysis includes:

- Main routine, output-file and plots generation from the found peaks.
  - See Listing B.1, for the energy calibration routine.
  - See Listing B.2, for the efficiency calibration routine.
- Subroutine, see Listing B.3. Fitting to the probably density of a generalized Gaussian distribution. Determined parameters: mean (μ), standard deviation (σ) with a 95% confidence level, peak area, background height and goodness-of-fit R^2.

Listing B.1: Main MATLAB script for the energy calibration. Generates an output-file from the found peaks. Software used: MATLAB 2019R5.

```
%%%%%%%%%%%%%%%%%%%%%%%%%%%%%%%%%%%%%%%%%%%%%%%%%%%%%%%%%%%%%%%%%%%%%%%%%%%%%%%%
%-------------------------------Energy Calibration-------------------------------
%%%%%%%%%%%%%%%%%%%%%%%%%%%%%%%%%%%%%%%%%%%%%%%%%%%%%%%%%%%%%%%%%%%%%%%%%%%%%%%%
% Energy calibration script for the analysis of converted spectrums
% files from the CAMBERRA format .CNF to .txt, by using the 'cambio'
% software from US DOE (https://www.osti.gov//servlets/purl/1232481).
% 'cambio' Version: cambio_cl_linux_x86_d3_20191022
%
% Expected Output: "output"
% (:,1) Peak_centroid ; (:,2) Ch_error ; (:,3) R^2
%%%%%%%%%%%%%%%%%%%%%%%%%%%%%%%%%%%%%%%%%%%%%%%%%%%%%%%%%%%%%%%%%%%%%%%%%%%%%%%%
close all
clear
path = pwd ;  % mention your working path

%.TXT files
%filename='./energy/Cs137ECal';
%filename='./energy/Ra226ECal';
filename='./energy/Eu152ECal';
%filename='./energy/Ba133Ecal';
%filename='./energy/Am241ECal';

import=importdata(filename);
fullspectro=str2double(import.textdata((18:end),(1:3)));

sp=fullspectro(:,[1,3]); % full spectrum for analysis (channel, counts)

```

```
%-Peaks channel location and height using the Signal Processing Toolbox
[pks,locs] = findpeaks(sp(:,2),sp(:,1),'MinPeakHeight',120,'MinPeakProminence',100,'MinPeakDistance',20);

l=10; % Spected full peak width.
n=size(locs,1); %total number of peaks found

fit_out=zeros(n,9);
output=zeros(n,3); % Output variable

% Creating an output.txt FILE
fileID = fopen([filename '_output'],'wt');
fprintf(fileID,'Peak_centroid pk_err R^2\n');
FormatSpec=[repmat('%f ',1,size(output,2)) '\r\n'];

% Analysis for the k-th located peak
for k=1:n
spectra=fullspectro((locs(k)-l:locs(k)+l),[1,3]); %k-th peak

x=spectra(:,1);%k-th channel column
y=spectra(:,2);%k-th counts per column

% See sp_analysis.m for a detailed description
[fit_out(k,:),fit_pdf,x,y]=SP_analysis(x,y,spectra);

if fit_out(k,1)~=0 % Implies that R^2 from fit_output > 0.97

%%%%%%%%%%%%%%%%%%%%%%%%%%%%-OUTPUT files creation-%%%%%%%%%%%%%%%%%%%%%%%%%%%%
    output(k,:)=fit_out(k,[1,2,9]);
    fprintf(fileID,FormatSpec, output(k,:));
%%%%%%%%%%%%%%%%%%%%%%%%%%%%%%%%%%%%%%%%%%%%%%%%%%%%%%%%%%%%%%%%%%%%%%%%%%%%%%%

end %end if
end %end for
fclose(fileID);
close all
```

Listing B.2: Main MATLAB script for the efficiency calibration. Generates an output-file and plots from the found peaks. Software used: MATLAB 2019R5.

```
%%%%%%%%%%%%%%%%%%%%%%%%%%%%%%%%%%%%%%%%%%%%%%%%%%%%%%%%%%%%%%%%%%%%%%%%%%%
% -------------------------Efficiency Calibration-------------------------
%%%%%%%%%%%%%%%%%%%%%%%%%%%%%%%%%%%%%%%%%%%%%%%%%%%%%%%%%%%%%%%%%%%%%%%%%%%
% Efficiency calibration script for the analysis of converted spectrums
% files from the CAMBERRA format .CNF to .txt, by using the 'cambio'
% software from US DOE (https://www.osti.gov//servlets/purl/1232481).
% 'cambio' Version: cambio_cl_linux_x86_d3_20191022
%
% e : Energy/Channel factor
% l : Size ofhalf-ROI, in Ch.
% Expected Outputs
%
% TXT file output:
% (:,1) Energy (KeV); (:,2) En_error  ; (:,3) FWHM      ;
% (:,4) FWHM_error  ; (:,5) area      ; (:,6) area_error ;
% (:,7) BKG_height  ; (:,8) BKG_h_err ; (:,9) R^2        ;
% (:,10) Live_time  ; (:,11) mes_date
%
% PLOTS:
% plots showing: DATA, fitted fuction and the centroide of the peak.

%%%%%%%%%%%%%%%%%%%%%%%%%%%%%%%%%%%%%%%%%%%%%%%%%%%%%%%%%%%%%%%%%%%%%%%%%%
close all
clear
path = pwd ;  % mention working path

%Input .TXT coverted efficiency files
filename='./Ra226';
%filename='./Cs137';
%filename='./Ba133';
%filename='./Eu152';
%filename='./Co60';

import=importdata(filename);
fullspectro=str2double(import.textdata((18:end),(1:3)));

% full spectrum for the analysis, in channel vs. counts
sp=fullspectro(:,[1,3]);

sp((1:185),2)=zeros; %ignore peaks below ~50 keV.
```

```
41
42 e=0.272413; % Energy calibration factor
43 l=8; % half-ROI size in Ch.
44
45 %-Peaks channel location and height using the Signal Processing Toolbox
46 [pks,locs] = findpeaks(sp(:,2),sp(:,1),'MinPeakHeight',225,'
       MinPeakProminence',50,'MinPeakDistance',1);
47
48 n=size(locs,1); %total number of speaks found
49
50 date=char(import.textdata(8,2)); % date of the measurement
51 time=str2double(import.textdata(3,2));% Live time
52
53 fit_out=zeros(n,9); % peak infomation output variable
54
55 %Creating an output.txt FILE
56 fileID = fopen([filename '_output'],'wt');
57 fprintf(fileID,'Energy(KeV) En_err FWHM FWHM_err Area Area_err y0
       y0_err R^2 live_time date\n');
58 FormatSpec=['%.3f %.3f %.3f %.3f %.0f %.0f %.0f %.0f %.3f %.0f %s \r\n'
       ];
59
60 %Analysis for the k-th located peak
61 for k=1:n
62 spectra=fullspectro((locs(k)-l:locs(k)+l),[1,3]); %k-th peak full ROI
63
64 x=spectra(:,1)*e; % k-th peak ENERGY column
65 y=spectra(:,2);   % k-th peak counts column
66
67 % k-th peak analysis.
68 % See SP_analysis.m description for a detailed description.
69 [fit_out(k,:),fit_pdf,x,y]=SP_analysis(x,y,spectra);
70
71 fit_out(k,5)=fit_out(k,5)/e; %correction from the SP_analysis routine.
72 fit_out(k,6)=fit_out(k,6)/e; %correction from the SP_analysis routine.
73
74 if fit_out(k,1)>50 && fit_out(k,1)<2500 && fit_out(k,2)~=0
75 % fit_out(k,1)>75 && fit_out(k,1)<1800, consider only the peaks in
       between this energies values.
76 % fit_out(k,2)~=0% Implies R^2>0.97 from SP_analysis.m
77
78 %%%%%%%%%%%%%%%%%%%%%%-OUTPUT file and figures creation-%%%%%%%%%%%%%%%%%%%%%%
```

```
fprintf(fileID ,FormatSpec , fit_out(k ,:) ,time , date); %TXT file output

 figure(k)
 plot(fit_pdf , 'r', x,y, 'fit');
 hold on
 xline(fit_out(k,1));
 xlabel('Energy [keV]'),ylabel('Counts'), grid on;
 ylim([0 1.10*pks(k)]);
 legend('Spectrum', 'Fit',['E_0=' num2str(round(fit_out(k,1) ,2))]);
 hold off
 saveas(figure(k),fullfile(path ,[filename '_' num2str(round(fit_out(k
     ,1))) '_spectrum.png']));
%%%%%%%%%%%%%%%%%%%%%%%%%%%%%%%%%%%%%%%%%%%%%%%%%%%%%%%%%%%%%%%%%%%%%%%%%%%%%%%%%%%%%%%%%%%%%%%
end %end if
end %end for
fclose(fileID);
```

Listing B.3: Subroutine MATLAB function. For the fitting to the probably density of a generalized Gaussian distribution. Determined parameters: mean (μ), standard deviation (σ), peak area, background height and goodness-of-fit R^2. Software used: MATLAB 2019R5.

```
function [out,pdf,x,y]= SP_analysis(x,y,spectra)
%%%%%%%%%%%%%%%%%%%%%%%%%%%%%%%%%%%%%%%%%%%%%%%%%%%%%%%%%%%%%%%%%%%%%%%%%%%%%%%%
%-----------------------------Analysis of the k-th peak-----------------------------
%%%%%%%%%%%%%%%%%%%%%%%%%%%%%%%%%%%%%%%%%%%%%%%%%%%%%%%%%%%%%%%%%%%%%%%%%%%%%%%%
%       u : Centroid peak value
%       s : Standard deviation
%       a : Estimated area under the peak
%      y0 : Estiamted background height
%% [pdf,gof] = fit(x,y,'user_funtion')
%           pdf : Output name from the fitting object
%           gof : Returns goodness-of-fit statistics values
% "out" values
% (:,1) Peak_centroide; (:,2) Pk_error  ; (:,3) FWHM;
% (:,4) FWHM_error    ; (:,5) Area      ; (:,6) Area_error ;
% (:,7) BKG_height    ; (:,8) BKG_h_err ; (:,9) R^2
%%%%%%%%%%%%%%%%%%%%%%%%%%%%%%%%%%%%%%%%%%%%%%%%%%%%%%%%%%%%%%%%%%%%%%%%%%%%%%%%
xmax=max( x( find( y==max(y))));% Centroid peak initial guess
area=sum(spectra(:,2));% Area under the curve INITIAL GUESS.

% Fitting function 'f': Generalized gaussian function.
f=fittype(@(a,s,u,y0, x) y0 + (a ./(s .*sqrt(2 .* pi))) .* exp( -0.5 .*
    ((x-u)/s).^2) );

pin=[area,0.4,xmax,1]; % a,s,u,y0 INTIAL GUESS values.

[pdf,gof] = fit (x, y, f, 'StartPoint', pin);

if (gof.rsquare>0.97) %R^2 from the fit > 0.97

% Array with the upper and lower limits of the fitting parameters with
    a confidence interval of 95%
ci = confint(pdf,0.95);

out(1,1)=pdf.u; % Peak Centroide value
out(1,2)=abs(ci(2,3)-ci(1,3));

out(1,3)=abs(2.35482*pdf.s); %FWHM
```

```
36 out(1,4)=abs(2.35482*(ci(2,2)-ci(1,2)));
37
38 out(1,5)=abs(pdf.a); %Area under the peak
39 out(1,6)=abs(ci(2,1)-ci(1,1));
40
41 out(1,7)=(pdf.y0); %BKG height in counts
42 out(1,8)=abs(ci(2,4)-ci(1,4));
43
44 out(1,9)=gof.rsquare; %R^2 value from the fitting
45
46 else %if R^2<0.97 printout a zeros vector
47 out(1:9)=zeros;
48 end
```

B.3.1 Routine output, efficiency calibration

The *efficiency calibration* main routine outputs are presented.

Table B.1: Efficiency calibration main routine output text-file from the ^{137}Cs data: "Cs137_output.txt".

Energy(KeV)	En_err	FWHM	FWHM_err	Area	Area_err	y0	y0_err	R∧2	live_time	date
661.628	0.034	1.306	0.099	6356	552	3	41	0.998	2000	2021-Aug-10

Table B.2: Efficiency calibration main routine output text-file from the ^{241}Am data: "Am241_output.txt".

Energy(KeV)	En_err	FWHM	FWHM_err	Area	Area_err	y0	y0_err	R∧2	live_time	date
26.267	2.103	0.326	14.77	203	1895	153	309	0.21	2000	2021-Aug-10
59.444	0.004	0.744	0.009	40270	503	36	49	1.000	2000	2021-Aug-10

Table B.3: Efficiency calibration main routine output text-file from the ^{152}Eu data: "Eu152_output.txt".

Energy(KeV)	En_err	FWHM	FWHM_err	Area	Area_err	y0	y0_err	R∧2	live_time	date
121.642	0.016	0.823	0.037	25713	1004	0	0	0.999	4000	2021-Aug-10
244.556	0.042	0.997	0.1	5225	454	0	0	0.994	4000	2021-Aug-10
344.151	0.013	1.05	0.031	13312	345	0	0	0.999	4000	2021-Aug-10
778.855	0.053	1.499	0.126	3497	254	0	0	0.995	4000	2021-Aug-10
964.015	0.043	1.564	0.1	3215	179	0	0	0.997	4000	2021-Aug-10
1085.823	0.083	1.723	0.195	2146	210	0	0	0.989	4000	2021-Aug-10
1112.064	0.075	1.671	0.177	2686	246	0	0	0.99	4000	2021-Aug-10
1408.013	0.066	1.766	0.157	3335	256	0	0	0.993	4000	2021-Aug-10

Table B.4: Efficiency calibration main routine output text-file from the $^{133}\mathrm{Ba}$ data: "Ba133_output.txt".

Energy(KeV)	En_err	FWHM	FWHM_err	Area	Area_err	y0	y0_err	R∧2	live_time	date
80.884	0.052	0.795	0.123	10927	1462	0	0	0.987	2000	2021-Aug-10
276.26	0.057	1.061	0.133	1543	168	0	0	0.99	2000	2021-Aug-10
302.726	0.019	1.019	0.046	3653	142	0	0	0.999	2000	2021-Aug-10
355.891	0.017	1.065	0.04	10441	340	0	0	0.999	2000	2021-Aug-10
383.762	0.055	1.094	0.13	1423	146	0	0	0.992	2000	2021-Aug-10

Table B.5: Efficiency calibration main routine output text-file from the $^{226}\mathrm{Ra}$ data: "Ra226_output.txt".

Energy(KeV)	En_err	FWHM	FWHM_err	Area	Area_err	y0	y0_err	R∧2	live_time	date
186.087	0.019	0.852	0.051	8922	540	357	49	0.999	4000	2021-Aug-10
241.859	0.009	0.941	0.023	16667	422	223	37	1	4000	2021-Aug-10
295.095	0.005	0.999	0.013	36553	514	201	43	1	4000	2021-Aug-10
351.868	0.998	1.097	0.614	68019	173402	233	40	0.999	4000	2021-Aug-10
609.263	0.012	1.263	0.035	49970	1560	83	117	1	4000	2021-Aug-10
768.344	0.036	1.387	0.109	4353	401	63	29	0.998	4000	2021-Aug-10
806.164	0.072	1.397	0.221	1131	210	57	15	0.991	4000	2021-Aug-10
934.071	0.051	1.522	0.166	2454	325	53	22	0.996	4000	2021-Aug-10
1120.282	0.033	1.639	0.115	10182	901	38	59	0.998	4000	2021-Aug-10
1238.111	0.039	1.779	0.15	3839	430	21	27	0.998	4000	2021-Aug-10
1764.526	0.049	2.025	0.227	7099	1153	19	68	0.997	4000	2021-Aug-10

Table B.6: Efficiency calibration main routine output text-file from the $^{60}\mathrm{Co}$ data: "Co60_output.txt".

Energy(KeV)	En_err	FWHM	FWHM_err	Area	Area_err	y0	y0_err	R∧2	live_time	date
1173.197	0.039	1.652	0.138	3632	385	7	25	0.998	2034	2021-Aug-10
1332.514	0.075	1.725	0.276	3103	646	6	41	0.992	2034	2021-Aug-10

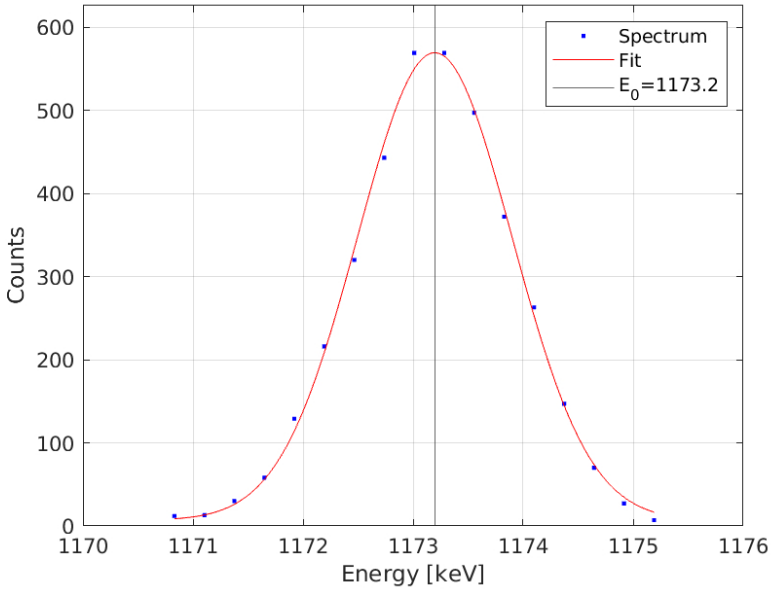

(a) Spectrum at 1173 KeV.

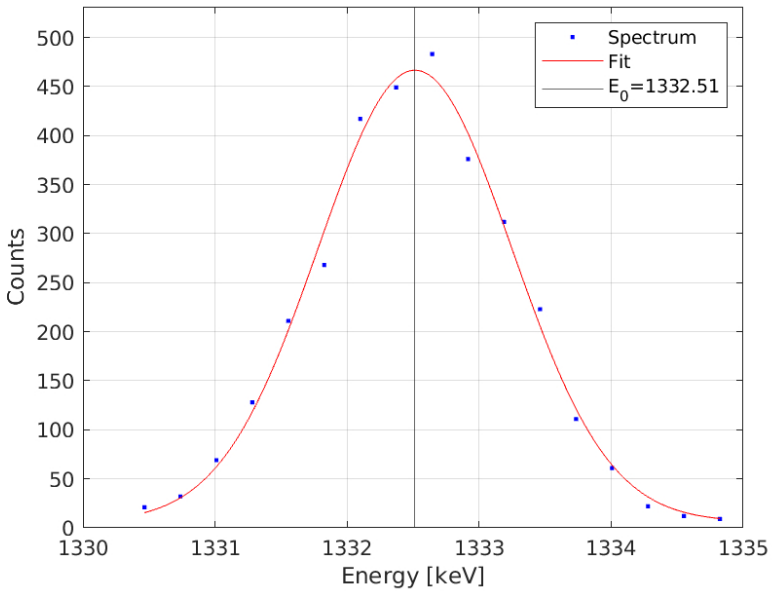

(b) Spectrum at 1332 KeV.

Figure B.6: Efficiency calibration main routine output figures from the ^{60}Co data.

Appendix C

Fit results

The following fitting results are presented:

- U-ZrH attenuation coefficient. See Listing C.1 and Figure 4.6.
- SS 304 attenuation coefficient. See Listing C.2 and Figure 4.7.
- Dry-air at sea level attenuation coefficient, using $\rho = 1.275 \times 10^{-3}$ (g/cm^3). See Listing C.3.
- water attenuation coefficient, using $\rho = 1.00$ (g/cm^3). See Listing C.4.
- Detector energy calibration. See Listing C.5 and Figure 5.3.
- Detector efficiency calibration. See Listing C.6 and Figure 5.4.

Listing C.1: Fitting results for the U-ZrH attenuation coefficient. Software used: QtiPlot 0.9.8.9 svn 2288.

```
Non-linear Fit of dataset: Table_U-ZrH, using function: A1*exp(-x/t1)+
    A2*exp(-x/t2)+y0
Weighting Method: No weighting
Scaled Levenberg-Marquardt algorithm with tolerance = 0.0001
From x = 5.0000000000000e-01 to x = 5.0000000000000e+00
A1 = 1.4981728329333e+00 +/- 2.5667333448330e-01
A2 = 4.1556198768611e-01 +/- 4.6742861696503e-02
t1 = 2.1890195045096e-01 +/- 2.6797879912506e-02
t2 = 9.6104853538193e-01 +/- 7.4048873435928e-02
y0 = 2.1049945462284e-01 +/- 2.3328733363515e-03
--------------------------------------------------------------------------------
Chi^2/doF = 5.5770729102001e-06
R^2 = 0.9997790216394
Adjusted R^2 = 0.9995948730056
RMSE (Root Mean Squared Error) = 0.00236158271297
RSS (Residual Sum of Squares) = 3.90395103714e-05
--------------------------------------------------------------------------------
Iterations = 18
Status = success
--------------------------------------------------------------------------------
```

Listing C.2: Fitting results for the SS 304 attenuation coefficient. Software used: QtiPlot 0.9.8.9 svn 2288.

```
Non-linear Fit of dataset: Table_SS(304), using function: A1*exp(-x/t1)
    +A2*exp(-x/t2)+y0
Weighting Method: No weighting
Scaled Levenberg-Marquardt algorithm with tolerance = 0.0001
From x = 5.0000000000000e-01 to x = 5.0000000000000e+00
A1 = 4.1462541315204e-01 +/- 2.7071841617389e-02
A2 = 5.5325664496264e-01 +/- 1.6310123053161e-02
t1 = 1.3920983578276e+00 +/- 7.4250392588271e-02
t2 = 3.5835912179358e-01 +/- 2.8623865100671e-02
y0 = 2.3676952975623e-01 +/- 2.1522477093614e-03
--------------------------------------------------------------------------------
Chi^2/doF = 9.7397543395717e-07
R^2 = 0.9999660717949
Adjusted R^2 = 0.9999377982906
RMSE (Root Mean Squared Error) = 0.0009869019373561
RSS (Residual Sum of Squares) = 6.8178280377e-06
```

```
16 ----------------------------------------------------------------------
17 Iterations = 94
18 Status = success
19 ----------------------------------------------------------------------
```

Listing C.3: Fitting results for dry-air at sea level attenuation coefficient. Software used: QtiPlot 0.9.8.9 svn 2288.

```
1  Non-linear Fit of dataset: mu_air, using function: y0+A*exp(-x/t)
2  Weighting Method: No weighting
3  Scaled Levenberg-Marquardt algorithm with tolerance = 0.0001
4  From x = 5.000000000000000e-01 to x = 3.000000000000000e+00
5  A = 1.163050315515671e-04 +/- 2.797332545048948e-06
6  t = 9.356254760088659e-01 +/- 5.459712907443973e-02
7  y0 = 4.183352742484886e-05 +/- 1.667462445572188e-06
8  ----------------------------------------------------------------------
9  Chi^2/doF = 1.141689184445767e-12
10 R^2 = 0.998385746576642
11 Adjusted R^2 = 0.997175056509123
12 RMSE (Root Mean Squared Error) = 1.06849856548606e-06
13 RSS (Residual Sum of Squares) = 5.70844592222884e-12
14 ----------------------------------------------------------------------
15 Iterations = 4
16 Status = success
17 ----------------------------------------------------------------------
```

Listing C.4: Fitting results for water attenuation coefficient. Software used: QtiPlot 0.9.8.9 svn 2288.

```
1  Non-linear Fit of dataset: mu_water, using function: y0+A*exp(-x/t)
2  Weighting Method: No weighting
3  Scaled Levenberg-Marquardt algorithm with tolerance = 0.0001
4  From x = 5.000000000000000e-01 to x = 3.000000000000000e+00
5  A = 1.011271948358569e-01 +/- 2.248839825546909e-03
6  t = 9.287064542632377e-01 +/- 4.900954946406285e-02
7  y0 = 3.682631912874770e-02 +/- 1.294383148628840e-03
8  ----------------------------------------------------------------------
9  Chi^2/doF = 7.894612558092721e-07
10 R^2 = 0.998185441688644
11 Adjusted R^2 = 0.997278162532966
12 RMSE (Root Mean Squared Error) = 0.000888516322759055
13 RSS (Residual Sum of Squares) = 5.52622879066491e-06
14 ----------------------------------------------------------------------
```

```
Iterations = 4
Status = success
--------------------------------------------------------------------------------
```

Listing C.5: Fitting results for the energy calibration. Software used: QtiPlot 0.9.8.9 svn 2288.

```
Non-linear Fit of dataset: En_cal, using function: m*x+b
Weighting Method: No weighting
Scaled Levenberg-Marquardt algorithm with tolerance = 0.0001
From x = 2.9678000000000e+02 to x = 2.1813000000000e+02
b = 1.6128725799862e-01 +/- 1.4351357056681e-02
m = 2.7241299822901e-01 +/- 5.2478808175147e-06
--------------------------------------------------------------------------------
Chi^2/doF = 1.9728334547744e-03
R^2 = 0.9999999914643
Adjusted R^2 = 0.9999999906883
RMSE (Root Mean Squared Error) = 0.04441658985981
RSS (Residual Sum of Squares) = 0.04537516945981
--------------------------------------------------------------------------------
Iterations = 2
Status = success
--------------------------------------------------------------------------------
```

Listing C.6: Fitting results for the efficiency calibration. Software used: QtiPlot 0.9.8.9 svn 2288.

```
Non-linear Fit of dataset: Table1_eff-intr, using function: a0+a1*ln(x
    /1400)+a2*ln(x/1400)^2+a3*ln(x/1400)^3
Weighting Method: No weighting
Scaled Levenberg-Marquardt algorithm with tolerance = 0.0001
From x = 6.616280000000000e+02 to x = 1.332514000000000e+03
a0 = 6.521938730638986e-02 +/- 3.721546109434949e-03
a1 = -5.452271928808760e-02 +/- 1.636171728697593e-02
a2 = 4.426450163647222e-02 +/- 1.769554957110380e-02
a3 = 6.727988717629377e-03 +/- 4.996748026604047e-03
--------------------------------------------------------------------------------
Chi^2/doF = 7.677277818841558e-05
R^2 = 0.992651320814131
Adjusted R^2 = 0.989979073837452
RMSE (Root Mean Squared Error) = 0.00876200765740453
RSS (Residual Sum of Squares) = 0.000921273338260987
--------------------------------------------------------------------------------
```